Developments in preclinical cancer imaging: innovating the discovery of therapeutics

James R. W. Conway[1], Neil O. Carragher[2] and Paul Timpson[1]

Abstract | Integrating biological imaging into early stages of the drug discovery process can provide invaluable readouts of drug activity within complex disease settings, such as cancer. Iterating this approach from initial lead compound identification *in vitro* to proof-of-principle *in vivo* analysis represents a key challenge in the drug discovery field. By embracing more complex and informative models in drug discovery, imaging can improve the fidelity and statistical robustness of preclinical cancer studies. In this Review, we highlight how combining advanced imaging with three-dimensional systems and intravital mouse models can provide more informative and disease-relevant platforms for cancer drug discovery.

Phenotypic screening
Assay systems that enable quantifiable measurements of cell phenotype or function that can be used to guide compound selection or iterative chemical design, often in the absence of any prior knowledge of an intended drug target.

[1]*Garvan Institute of Medical Research and The Kinghorn Cancer Centre Sydney, St Vincent's Clinical School, Faculty of Medicine, University of New South Wales, New South Wales 2010, Sydney, Australia.*
[2]*Edinburgh Cancer Research UK Centre, MRC Institute of Genetics and Molecular Medicine, University of Edinburgh, Edinburgh, EH4 2XR, UK.*
Correspondence to P.T. and N.O.C.
e-mails: p.timpson@garvan.org.au; n.carragher@ed.ac.uk
doi:10.1038/nrc3724
Published online 17 April 2014

Despite the high number of promising lead compounds that enter the drug discovery pipeline, several challenges must be overcome to support their clinical application (FIG. 1). Owing to unforeseen side effects or lack of efficacy in live disease tissue, a high attrition rate of candidate drugs remains during development[1]. Limited efficacy often results from inefficient inhibition of the intended drug target and/or compensatory or redundant disease mechanisms. Similarly, a lack of dynamic or reversible readouts of drug action in more complex disease settings may contribute to the high attrition rates that we observe when drugs enter clinical trials[2–4]. To minimize late-stage failure, we must improve early drug discovery strategies and preclinical modelling to better mimic and thereby predict clinical response in the target tissue environment[3–8].

Target-based screening approaches are those in which rational molecular targets that are hypothesized to have a role in disease have been the focus of drug design. This has been the predominant strategy operated by the pharmaceutical and biotechnology industry for the past 25 years and represents the vast majority of drug discovery projects. In contrast, automated image-based phenotypic screening technologies are those in which the identification and optimization of chemical leads are based on cellular phenotypic or functional endpoints, rather than target potency alone (reviewed in REF. 9). Interestingly, a retrospective analysis of all drugs approved by the US Food and Drug Administration (FDA) between 1999–2008 indicated that of first-in-class small molecule medicines approved, 37% (28 drugs) were initially identified by a phenotypic discovery approach, relative to 23% (17 drugs) identified by target-directed drug discovery[1,10]. Thus, complementary to target-directed approaches, high-throughput phenotypic image-led drug discovery may present a productive methodology for the identification of novel first-in-class medicines.

In this Review, we describe how the application of emerging advanced high-throughput *in vitro* and intravital imaging technologies can be integrated into standard drug project operating models (DPOMs) (FIG. 1). We highlight current fluorescence-based technologies, as well as biosensors, and how these technologies can provide quantitative information on drug activity, with high spatial and temporal resolution. We show how mimicking the three-dimensional (3D) microenvironment of disease can be used to bridge the gap between *in vitro* and *in vivo* drug development, and we demonstrate the power of real-time, non-invasive and repeated intravital imaging approaches for innovation of both target-based and phenotypic-based drug discovery strategies.

Advanced image-based screening techniques

Image-based phenotypic screening approaches can provide high-throughput *in vitro* readouts of key parameters that represent commonly desired properties of anticancer therapies. These phenotypic readouts can include, for example, changes in morphology[11] (including cytoskeletal remodelling[12]), proliferation[13], migration[14], cellular trafficking[15] and cell cycle progression[16].

Key points

- Advanced fluorescence-based imaging, three-dimensional intermediate systems and intravital mouse models can be integrated into the standard drug project operating model (DPOM) to better inform the development and selection of new candidate drugs.
- Intermediate systems provide initial three-dimensional imaging early in the drug discovery process to support translational cancer research in more physiologically relevant *in vitro* settings and identify deficient or ineffective drug strategies earlier in the drug discovery pipeline.
- *In vivo* advanced imaging techniques can be used to assess more complex questions, such as transient protein–protein interactions or molecular, cell or tissue-specific dynamics in response to drug treatment in live tissue.
- Biosensors are now providing dynamic and reversible fluorescence-based readouts of drug targeting, allowing drug turnover, clearance and dissociation to be monitored in real-time.
- Stromal targeting of the tumour microenvironment is a vital aspect of cancer drug development, which can be quantified using advanced imaging techniques, such as second harmonic generation (SHG), third harmonic generation (THG) and fluorescence lifetime imaging microscopy (FLIM).
- Longitudinal imaging through intravital imaging windows can give quantitative functional information from repeated, non-invasive imaging and drug endpoint analysis in real-time.

First-in-class small molecule medicines
Newly approved medicines that have novel mechanisms of action, distinct from anything else on the market.

Target-directed drug discovery
A contemporary strategy for the identification and optimization of lead molecules and candidate drugs based on achieving high levels of potency and specificity against a nominated target that is implicated in disease progression.

The recent incorporation of more advanced fluorescence-based assays into high-throughput image-based drug discovery platforms is now providing less descriptive, highly dynamic, fluorescence readouts in target cells, both *in vitro* and, more recently, using intravital imaging *in vivo* (TABLE 1). Examples of these dynamic fluorescence readouts include bimolecular fluorescence complementation (BiFC), fluorescence resonance energy transfer (FRET; also known as Förster resonance energy transfer), photoswitching or photoactivation, fluorescence recovery after photobleaching (FRAP) and fluorescence lifetime imaging microscopy (FLIM).

BiFC. BiFC enables measurements to be recorded for protein–protein interactions in which two halves of a fluorophore are intramolecularly linked to separate proteins of interest. The irreversible re-association of fluorescent protein fragments can then be used to detect whether an interaction takes place between tagged proteins of interest, as implied through complementation of the whole fluorophore (TABLE 1). In this way, BiFC has been used to investigate transmembrane domain receptor signalling[17], autophagy[18], cellular stress[19] and, recently, *in vivo* protein–protein interactions[20]. In addition, BiFC can be used to monitor protein degradation and stability by using fluorescent-protein fragments fused to ubiquitin and a substrate protein. As in other BiFC studies, the association of ubiquitin to its substrate protein brings the fluorescent protein fragments together and generates a fluorescent signal that can be used for real-time tracking of ubiquitylation and protein degradation[21]. This can be used in early drug treatment studies, when ubiquitin-mediated degradation and other post-transcriptional modifications, such as sumoylation, can affect efficacy[21,22].

FRAP and photoswitching or photoactivation. FRAP and photoswitching or photoactivation of fluorescent proteins tagged to a protein of interest have been used to investigate key biological processes in diseases such as cancer. To carry out FRAP analyses, the specific regions of interest, which are marked with fluorescent proteins, are photobleached and the recovery rate of the fluorescence signal is monitored. FRAP readouts have allowed the quantitative assessment of membrane dynamics[23–29], subcellular diffusion analysis[30,31], chromatin association[32–37] and sub-nuclear domain exchange or shuttling in response to drug treatment[38]. Furthermore, FRAP has been used to measure protein–protein interactions[39–41], identify multiprotein complexes[35,42] and demonstrate DNA and protein interactions during different stages of the cell cycle[43–45]. FRAP-based approaches have also been used to monitor the subcellular stability of molecules that are known to hold tumour cell populations together, such as E-cadherin, in the context of anti-metastatic drug treatment[26–29] or in response to endocytic or integrin inhibition *in vivo*[25].

Photoswitching or photoactivation makes use of photoswitchable or photoactivatable fluorescent proteins. After activation or switching to a different colour, tagged proteins or cells of interest can be tracked, thereby giving quantifiable measurements of cellular dynamics over time. Photoswitching or photoactivation has been used to assess cellular motility[46–48], morphology[49], the transport of cytosolic proteins[50] or to track endocytic or vesicular trafficking events[51,52]. Photoswitching or photoactivation technology has been used *in vivo* to tag and track individual tumour cell populations using repeated imaging of the same area over time[53,54]. In this way, the effects of drugs on cell motility, mode of invasion and the persistence of movement can be monitored over short-to-long time periods in distinct locations within the tumour mass. Photoactivation has also been used to monitor *in vivo* changes in plasma membrane dynamics at subcellular resolution, which have a vital role in cell motility and invasion[24–26].

FRAP and photoswitching or photoactivation have also been applied in 3D systems to monitor early tumour dissociation dynamics or the activity and localization of matrix metalloproteinases (MMPs) during cell invasion and drug administration[55,56]. Therefore, the application of these technologies provides easily accessible fluorescence readouts for monitoring protein reactions or to track cells over extended time courses. This could promote their application in early drug development programmes, from hit identification to lead optimization within the DPOM (FIG. 1; TABLE 1).

FRET. Similar to BiFC, FRET can be used to measure protein–protein interactions. FRET refers to the non-radiative transfer of excited state energy between colocalized donor and acceptor fluorophores[57,58]. As this occurs when fluorophores are in close proximity (~5 nm), FRET signifies a molecular interaction between fluorescently labelled proteins. This lends FRET to studies of intramolecular and intermolecular protein interactions and FRET has been used to monitor cell–cell adhesion[59,60], cell invasion[61], MMP activity[62–64], apoptosis[65] and for real-time monitoring of cell division[66–68]. Importantly, unlike BiFC, FRET is reversible and therefore allows the dissociation of

Anisotropy
The anisotropy of a molecule is assessed through the simultaneous measurement of orthogonally polarized fluorescence relative to the polarization of the excitation light. Factors that determine the degree of anisotropy are protein mobility and molecular orientation. As a consequence, anisotropy can be used as a powerful and sensitive readout for binding and screening assays of protein behaviour and interactions.

the interaction to be measured. For example, a reversible FRET biosensor has recently been used to monitor both the inactivation and reactivation kinetics of SRC kinase in live tumours after drug clearance, thereby helping to inform and optimize the frequency of drug administration for maximum benefit[69]. FRET can therefore be used to monitor reversible reactions or loss of drug-target potency over time, and it is ideally suited to the lead optimization and pharmacodynamic arm of the DPOM[58,70–73] (FIG. 1; TABLES 1,2). Furthermore, photoactivatable fluorescent proteins are now facilitating photoactivation–FRET through both intramolecular biosensor development[74] and intermolecular interactions[75,76], in which the donor or acceptor fluorophores are only active upon photoactivation (TABLE 1). In this way, the fluorescence readout or subcellular application of FRET can be dynamically controlled, while reducing the effects of phototoxicity.

High-speed FLIM–FRET. More recently, techniques that enable the rapid quantification of fluorescence have facilitated high-speed FRET analysis. This is suitable for high-throughput molecular or chemical screening for early hit and lead identification within the DPOM (FIG. 1). One such technique is FLIM, which has been used to measure the excited state lifetime of the donor fluorophore in a FRET interaction. The donor lifetime is reduced when fluorophores are in close proximity (~5 nm) and, thus, can provide a precise measurement for drug activity, protein interactions and protein activation both *in vitro* and *in vivo*[77–82]. In addition, FLIM measurements of FRET are insensitive to artefacts caused by variations in fluorescent protein levels, which can be problematic for standard FRET microscopy (reviewed in REFS 3,83–86). Furthermore, an advantage of FLIM over other methods is the use of fluorescence lifetime measurements of a target as an internal control before drug treatment. This lends FLIM–FRET to studies of drug treatment in more complex *in vivo* settings, where the application of FLIM to measure FRET has successfully been applied with high spatial resolution. Thus, FLIM–FRET is particularly appropriate to those treatments focused on the invasive borders of tumours, where both immune[87–90] and stromal[91,92] interactions are reportedly increased. Advances in this field have led to the development of high-speed FLIM–FRET to measure FRET interactions, and this can be applied in an automated high-throughput manner[78]. For example, high-speed FLIM was used to simultaneously monitor RAS GTPase activation (upon epidermal growth factor stimulation) with Ca^{2+} signalling[93]. This, along with the high-throughput FLIM identification of tyrosine phosphorylation feedback networks in breast cancer[79], highlights the potential application of FLIM for uncovering redundant or compensatory signalling events in response to various drug treatment regimens, during the target validation to optimization stages of drug development (FIG. 1).

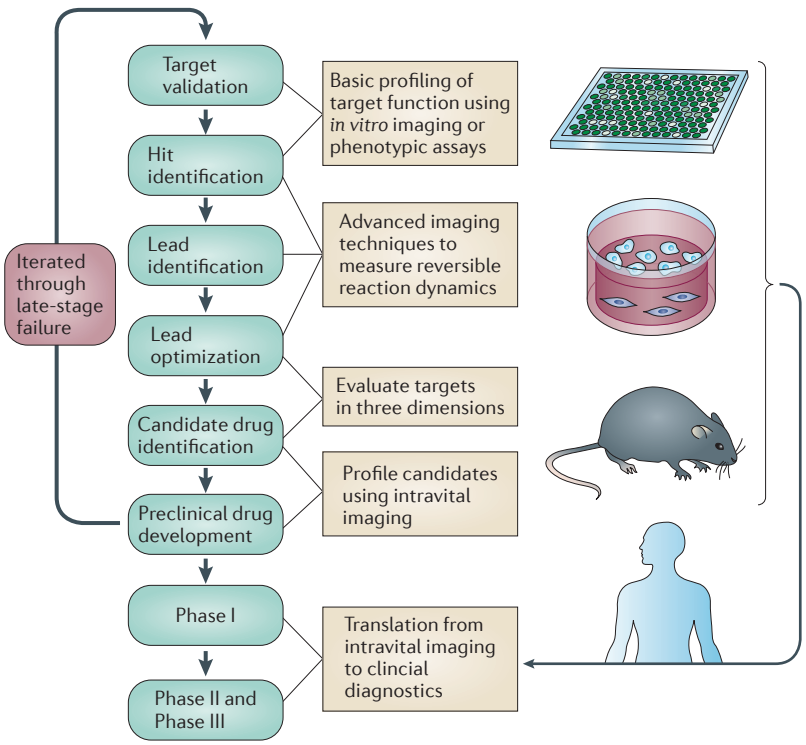

Figure 1 | **Applications of image-based high-content screening and intravital imaging increase the value of core elements of the drug project operating model (DPOM).** A workflow that shows when advanced preclinical imaging may add value to drug discovery, including initial target validation, hit and lead identification, lead optimization, drug nomination, preclinical drug development and Phase I, II and III clinical drug trial designs.

Anisotropy. Further to the applications of FLIM–FRET is anisotropic imaging. The anisotropy of a molecule is assessed through the simultaneous measurement of polarized fluorescence in perpendicular and parallel directions. Anisotropy is affected by various factors, such as protein mobility and molecular orientation. Such anisotropic measurements can be recorded on both confocal and wide-field microscopes and are progressing imaging studies towards high-throughput settings that are suitable for hit and lead identification phases of the DPOM (FIG. 1). Anisotropy has been used to assess key processes, such as chromatin compaction following drug treatment[94], cell membrane fluidity[95] and DNA digestion by nucleases[96]. In addition, anisotropy is well suited to the measurement of Homo-FRET (a process where FRET occurs between two or more identical fluorophores) and has been used to monitor oligomerization of specific protein targets, such as glycosylphosphatidylinositol (GPI)-anchored proteins, in living cells[97]. Such measurements of clustering or self-association of proteins tagged with fluorophores may give functional information at the single-molecule level during drug treatment, and they could offer greater precision in the investigation of therapies that target the dissociation of molecular clustering. The recent use of automated fluorescence anisotropy imaging in a Hetero-FRET protein–protein interaction assay (a process in which FRET occurs between two non-identical fluorophores) showed the advantages of higher dynamic range and faster speed of anisotropic imaging compared to standard FLIM–FRET microscopy[98].

Table 1 | **Settings, advances and challenges in drug discovery imaging**

Technique	Advantages in drug discovery imaging	Challenges in drug discovery imaging
BiFC 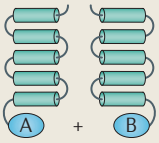	• Stable monitoring of protein–protein interactions • Maintains cellular spatiotemporal context of protein interaction networks • Low background • High specificity • Simultaneous detection of multi-protein complexes • Can monitor protein modifications (e.g. ubiquitylation or sumoylation) • Facilitates monitoring of protein stability and degradation rate over a long time course with spatiotemporal resolution (e.g. UbFC)	• Irreversible process that cannot monitor loss of response (e.g. upon drug treatment) • Toxicity or mislocalization due to overexpression of proteins • Potential interference of interactions via fusion protein • Exogenous expression of tagged fusion proteins may show distinct turnover rates and therefore altered degradation profiles relative to endogenous counterparts
FRAP 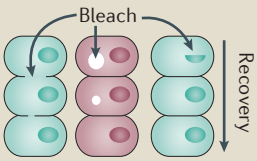	• Capacity to measure specific protein–protein interactions, including strength and stability at the subcellular level *in vitro* and *in vivo* • Measures the immobile fraction and the diffusion coefficient of protein targets • Precise analysis of stoichiometry and kinetics of macromolecular interactions • Identification of specific post-translational modifications and peptide motifs that govern molecular interactions • Design of functional assay endpoints (e.g. DNA damage response) that are suitable for monitoring drug intervention studies	• Low throughput and biased sampling of regions of interest • Stability of the region of interest *in vivo* • Need to account for bleaching spot sizes and the number of bleach scans • Normalization with post-bleach profile required • Identification of specific molecular components that dictate diffusion and interaction dynamics of tagged proteins in cells
Photoswitching or photoactivation 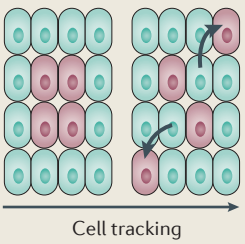	• Track cell mobility within the same tissue or distant locations (e.g. imaging and monitoring metastasis formation or drug response) • Monitor intracellular vesicular trafficking events • Monitor subcellular protein turnover and diffusion • Tracking of cell division and morphology changes • Observation of post-translational modification and degradation • Tracking of immune responses • Improved subcellular resolution and reduced phototoxicity to monitor protein–protein interactions when combined with FRET (photoactivation–FRET)	• Intrinsic blinking can lead to over-counting • Incomplete photoactivation or photoswitching may lead to loss of sensitivity • Protein oligomerization may introduce artifacts • Short wavelength light commonly used for photoactivation and photoswitching can induce phototoxicity in cells
FRET 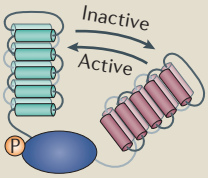	• Reversible interactions can be measured • Distinct drug targets and redundant mechanisms can be measured simultaneously • Can be used to measure donor lifetime • Increasing availability of intramolecular biosensors (see TABLE 2)	• Requires careful control of expression levels and ratio of proteins of interest • Fluorescent proteins with multiexponential decay curves may require dual measurements • Gentically engineered mouse models expressing FRET biosensors require careful selection of promotor or expression level for physiologically relevant tissue and lineage-specific expression

BiFC, bimolecular fluorescence complementation; FRAP, fluorescence recovery after photobleaching; FRET, fluorescence resonance energy transfer; P, phosphorylation; UbFC, ubiquitin-mediated fluorescence complementation.

FRET-based biosensors and drug-target readouts. In many preclinical studies, plasma drug concentrations are used as a surrogate to read out pharmacokinetic parameters, such as drug perfusion, delivery and retention. Although important, plasma drug concentrations cannot measure other factors that influence drug efficiency. These factors include target inactivation within the tumour cells or target tissues, as well as changes in the microenvironment that influence drug penetration of solid tissues, such as tumour–stromal interactions and extracellular matrix (ECM) relaxation. In line with this demand, FRET-based biosensors allow dynamic readouts of drug activity within target cells. Presented in TABLE 2 is a non-exhaustive list of intramolecular FRET-based biosensors with potential *in vivo* application for cancer research and drug discovery. These have been broadly classed into five themes: cleavage-based, substrate-based, binding-domain-based, and tag- or sensitivity-based biosensors.

Cleavage-based biosensors are those in which the biosensor itself is irreversibly cleaved by the protein in question, such as those describing membrane-type-1 MMP (MT1MMP; also known as MMP14)[62–64,99,100] and caspase 3 (REFS 71,101,102), for which loss of FRET upon cleavage of the biosensor can be used to measure activity. Cleavage-based sensors can read out numerous biological processes, including the activation of caspase 3 in cancer[71,101–103], which is important for the induction of apoptosis in response to both the extrinsic and intrinsic signalling pathways. Despite successful application of caspase 3 biosensors upon drug treatment *in vivo*[104,105], for which reversibility of the biosensor is

Extracellular matrix
(ECM). A reinforced composite of structural proteins that is primarily composed of collagen and tissue-specific inclusions (for example, fibronectin and laminin), as well as other metabolites secreted by cells. The ECM provides structural support and biochemical signals for multicellular tissue and organ systems.

not required after cell death, the irreversible loss of FRET post-cleavage means that subtle rates of cleavage could be 'drowned out' by the overwhelming presence of the active form of the biosensor, and inactivation of the relevant pathways upon drug treatment may be missed. Similarly, biological processes such as reversal of MMP activity upon drug treatment during invasion may be more difficult to monitor, owing to high

Table 2 | **Intramolecular FRET biosensors for *in vivo* cancer research***

Role	Target(s)	Pathway(s) relevant to cancer	Refs
Cleavage based			
Apoptosis	Caspase 3	• Caspase-dependent cell death • Inflammatory response	65,101,289,290
	Caspase 8	Apoptosis	291
Autophagy	ATG4A or ATG4B	Autophagosome biogenesis	292
ECM remodelling	MT1MMP	• Cell migration or invasion • Cell adhesion	62–64,99,100
Substrate based			
Cell division	CDK or cyclins	• Cell cycle progression • Proliferation	68
	PLK1	• DNA damage response • Cell cycle progression	293
Signal transduction	AKT (PKB)	• Survival • Metabolism • Apoptosis	107–110
	ERK	• Extracellular signal transduction • Proliferation • Differentiation	294
Cell–cell adhesion	FAK	• Cell adhesion • Proliferation • Integrin-mediated signalling cascades	59
	SRC	• Differentiation • Migration • Proliferation or survival	60,106
Immune system	CRKL (BCR–ABL)	• Oncogenic signal transduction • Proliferation • Survival • Cell adhesion	295
	ZAP70	• Signal transduction • TCR sensitivity	296
Binding domain based			
Motility	RHOA, RAC and CDC42	• Actin cytoskeletal remodelling • Cell–cell junction dynamics • Cell motility • ROS production • Proliferation	66,112
	RAS	• Tumour initiation • Proliferation • Differentiation	111
Tag based			
Metabolism	ATP	Intracellular energy transport	119
	Glutamate	Protein metabolism	118
	Glucose	Respiration	117
Sensitivity based			
Hypoxia	O_2	Energy homeostasis	121
Stress	pH	• Cytosolic homeostasis • Enzymatic processes • Cell cycle progression • Cell proliferation • Apoptosis induction	122,123

CDC42, cell division control protein 42; CDK, cyclin-dependent kinase; CRKL, CRK-like protein; ECM, extracellular matrix; FRET, fluorescence resonance energy transfer; FAK, focal adhesion kinase; MT1MMP, membrane-type-1 MMP; PKB, protein kinase B; ROS, reactive oxygen species; TCR, T cell receptor. *The table is non-exhaustive and used only to show the potential use of biosensors *in vivo*. We apologize for probes that are not cited owing to space constraints. A more extensive list can be found in REF. 141.

levels of the active form of the biosensor masking inactivation *in vivo*. Thus, when the biological process being addressed is reversible, reversible biosensors are desirable for dynamic drug studies.

Substrate-based biosensors are tagged proteins that are phosphorylated by the target in question. These biosensors function as surrogate markers for targets such as SRC[60,106], focal adhesion kinase (FAK)[59] or AKT[107–110] and provide advantages over cleavage-based probes, as they can be de-phosphorylated, thereby giving the reversibility that is required for dynamic drug studies. This type of biosensor was used to compare drug uptake with SRC inactivation using FLIM–FRET in live tissue[69]. In addition to monitoring drug turnover and clearance, this method revealed that SRC activity is increased at the invasive border of the tumour, thereby demonstrating spatiotemporal drug activity, which could not have been discovered using conventional techniques such as the measurement of plasma drug concentrations. A possible limitation of substrate-based biosensors is that they are based on the modification of a distinct downstream substrate and therefore infer upstream activation of the target of interest. Moreover, the phosphorylation of other effectors with potential relevance to the disease in question may be undetected using these probes alone.

In contrast to these downstream substrate-based probes, the RHO-family G proteins (Raichu series) are based on a specific RHO-family member being reversibly associated with an intramolecularly linked binding domain, in a GTP-bound form, termed here as 'binding-domain-based biosensors' (REFS 66,111,112). Although such biosensors provide important insight into key processes *in vivo*[113–116], RHO-family biosensors indicate the balance of guanine nucleotide exchange factor (GEF) to GTPase-activating protein (GAP) activity upstream of the target and, thus, also infer activity in this setting. Additionally, to maintain physiological relevance, strict control must be maintained for expression levels of all biosensors described here to avoid the sequestration or alterations of upstream and/or downstream signalling activity within cells.

Tag-based and sensitivity-based biosensors, such as those for glucose[117], glutamate[118] and ATP[119], could also provide spatiotemporal quantification of metabolic changes in cancer. These biosensors are dependent on a conformational change of a protein that has two domains tagged with a FRET pair. For example, the use of a dual-tagged glucose/galactose binding protein uses the glucose- or galactose-induced hinge-twist, which, upon binding, twists the fluorophores out of FRET range[117]. Similar to substrate-based and binding-domain-based biosensors, these biosensors may be limited by their indirect readout. Complementary validation of all types of biosensor readouts, such as parallel immunohistochemical staining after intravital imaging[120], could facilitate initial *in vivo* validation in this regard.

Sensitivity-based probes provide a dynamic method for detecting levels of intracellular components, such as oxygen[121] and pH[122,123]. These biosensors present a fast and reversible readout of target levels, again inferring activity, but without a loss of fluorescence efficiency or photostability, when compared with standard cyan fluorescent protein variants[124,125]. Blood flow, oxygen delivery and consumption, as well as hypoxia, are important aspects of *in vivo* cancer biology, and dual imaging of these factors that may influence tumour behaviour, with altered drug-target signalling, could potentially be co-monitored using these distinct but interdependent types of FRET biosensor readouts. Collectively, it is important to acknowledge that although these biosensors have great advantages over static images, to avoid data misinterpretation, the user must be aware of which specific molecular processes are read out by the FRET probes.

Furthermore, the recent application of multiple FRET-based biosensors within the same cell, with spectrally distinct fluorescent protein pairs, should allow the simultaneous detection of multiple cellular processes and improve the assessment of combination therapies that aim to counteract redundant or acquired resistance mechanisms[64,93,102,126,127]. Furthermore, these multicolour FRET assays are progressing towards high-throughput screens on cell arrays to monitor parallel and distinct molecular processes, within the same cell, thereby increasing their potential applications within the lead optimization arm of the DPOM[79–82] (FIG. 1).

As the use of biosensors has progressed, so has the development of transgenic mice that express these probes. Currently, transgenic mice that express intramolecular FRET biosensors for protein kinase A (PKA)[128], ERK[128], caspase 3 (REFS 104,105), Ca^{2+} (REFS 129–132), calpain[133] and cyclic AMP (cAMP)[134,135], as well as multiple G protein biosensor mice[115], have all been developed. Our recent generation of a RAC–FRET mouse, for example, allowed spatiotemporal monitoring of RAC activity in various organs within the body, in response to drug treatment[116]. Hence, biosensor mice are now able to be bred with cancer-type-specific disease models and thereby expand our knowledge of how these targets behave in a native host tissue, upon drug treatment. This is a substantial shift in the field and, once it is coupled with the optical window technology as discussed below, will enable real-time repeated imaging for use in dynamic drug discovery strategies (see BOX 1 for how biosensors are being improved for ease of use).

Imaging drug effects in cancer models

The development of fluorescent proteins and the technologies to detect them has run parallel with developments in 3D modelling and imaging *in vitro* and *in vivo*[136–141] (FIGS 2–4). 3D modelling has allowed the assessment of distinct modes of tumour invasion[142–145], the effects of hypoxia[146,147], ECM remodelling[69,148], receptor dimerization[149] and cancer–stromal cell interactions in co-cultures[150–154], which cannot always be observed in 2D culture.

3D modelling of disease: engineering more predictive models. 3D cell culture allows us to investigate whether drugs that aim to prime the tumour microenvironment could improve drug delivery and tumour cell sensitivity, when co-administered with anticancer therapies

Intravital imaging windows
Windows that are surgically implanted in a mouse to allow repeated, non-invasive imaging over a long time course.

in vivo. For example, findings within 3D spheroid cultures[155] and cell-derived matrices[156] have shown increased drug resistance in ovarian[157], liver[158], lung[159] and pancreatic cancer[160] compared with drugs tested in 2D systems[161].

3D modelling allows the study of several ECM factors that influence malignant progression by changing matrix architecture[69,148], stiffness[158,162–164] or porosity[153,165,166]. Mammary tumour cells, for example, show an increased invasive ability in areas governed by high, compared to low, biomechanical stress, driven by reciprocal ECM signalling *in vivo*[167,168]. Furthermore, targeting of the tumour–stromal compartment before chemotherapy has been shown to improve the perfusion of drugs into solid tumours *in vivo*[169–172]. The use of multiphoton-based second harmonic generation imaging (SHG imaging; a 'label-free' technique that is often used to assess the semi-crystalline architecture of the ECM using multiphoton microscopy) is facilitating the investigation of ECM attributes and allowing the drugs that affect them to be examined in a more direct and quantitative manner[173–175]. Using state of the art imaging systems and techniques, such as photoswitching or photoactivation, FRAP and FLIM–FRET, to examine drugs in more complex 3D *in vitro* and *in vivo* models could allow deficient or ineffective drugs to be identified earlier in the drug discovery pipeline, thereby streamlining validation before more complex *in vivo* assessment[176].

Intravital imaging in drug discovery. Low-resolution whole-body imaging techniques, such as luminescence-based approaches, have long been used in drug discovery to monitor tumour progression and regression rates from multiple tissue sites during drug treatment[177–180]. Although such amplified signalling techniques provide vital information from organs deep within the body, they have substantial disadvantages in their ability to provide single cell or subcellular detail to inform comprehensive drug discovery.

Intravital imaging has gained this cellular detail by tagging single cells, tissues and even subcellular compartments with fluorescent proteins, through direct labelling of cells before exogenous inoculation *in vivo* or by using tissue-specific promoters to drive expression within organs of interest[181–183]. These methods have been applied to monitor *in vivo* changes in invasion[61,142,184] and protrusion dynamics[114,185,186], and this has led to recent work that shows altered modes of invasion, such as cell streaming in patient-derived xenografts[187]. Similarly, tissue-specific expression of fluorescent proteins within mammary tissue[188,189], brain[190–192], pancreas[193,194], bladder[195], kidney[196], intestine[197–199] and skin[185,200–202] has been used to monitor distinct cancer behaviours upon drug treatment. Additionally, multi-cell-type imaging has revealed distinct stromal companions needed for processes that are fundamental to cancer, such as interstitial guidance by adipose cells during invasion[203–206], and simultaneous tagging of clonal progeny to track stem cells in intestinal or mammary tumours[53,189,197,207]. Multicellular tracing can therefore also be used to assess drug treatments that aim to target multiple cell populations in different cancers or organ types[46,189,197,198,208–213].

Real-time imaging has also advanced through the use of intravital imaging windows to monitor tumour progression in a longitudinal manner (FIG. 3). Skin-fold chambers (SFCs), for example, have been used for gross imaging of drug and MMP-derived breakdown of stromal components in tumours by SHG[214]; and cranial imaging windows (CIWs) have been used to analyse single stages of brain metastasis formation in real time[215] (FIG. 3). Mammary imaging windows (MIWs), have also been used in combination with orthotopic or tissue-specific mouse mammary tumour virus (MMTV)-derived green fluorescent protein (GFP)-expressing tumours to track intravasation and tumour motility in relation to the native tissue topology of the mammary gland[53,188,216] (FIG. 3). MIWs were later coupled with advanced imaging modes, such as photoswitching or photoactivation,

Box 1 | **Improvements in FRET biosensors**

The efficiency, brightness and *in vivo* applicability of intramolecular fluorescence resonance energy transfer (FRET; also known as Förster resonance energy transfer)-based biosensors is continuously being optimized. For example, new fluorescent protein variants are being developed with increased fluorescence efficiency, longer fluorescence lifetimes and monoexponential fluorescence decay for ease of analysis[271–274]. These longer lifetimes can help to address difficulties in assigning subtle decreases in fluorescence lifetime, which simplifies differentiation between FRET 'on/off' states to clarify distinct states of activity upon drug treatment. In addition, probes to allow deeper FRET imaging in disease have been developed using red/far-red type fluorophore pairs, such as LSSmOrange/mKate2 (REF. 102) and mKO/mCherry[275]. These improvements in fluorescent protein technology are also being coupled with changes in linker regions within the biosensor itself, such as for the Eevee series[107]. This is achieved through the use of long flexible linkers for a purely distance-dependent FRET interaction[107,276]. Notably, the 'chameleon' Ca^{2+} intramolecular FRET biosensors have undergone several stages of optimization. The first stage involved modification of the calmodulin Ca^{2+} binding domain affinity to allow additional subcellular application of these versatile biosensors[277,278]. Furthermore, improvements in the resistance of the FRET acceptor protein to environmental factors, predominantly to changes in pH[279–282], have led to the development of fluorescent protein variants with increased absorption of excited state energy and improved acceptor function *in vivo*[129]. Furthermore, both improved acceptor function and fluorescent protein dimerization affinity have an improved signal-to-noise ratio and an expanded dynamic range[129,283–287]. Finally, a novel application of FRET technology is the development of the Absense intramolecular FRET biosensors, in which a loss of FRET occurs upon antibody binding to the biosensor, thereby allowing the detection of antibody localization to a target tissue[288]. The application of these biosensors for the monitoring of antibody-based targeted therapies could lead to cross-disciplinary use of FRET and increase the number of applications of biosensors in antibody-driven drug discovery.

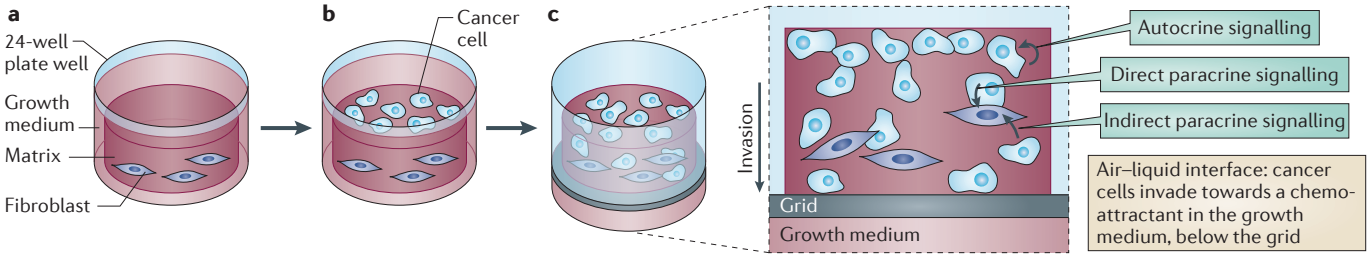

Figure 2 | **Engineering more predictive models for cancer research.** **a** | Schematic of a three-dimensional organotypic assay, whereby co-cultured fibroblasts are embedded in a collagen I matrix (organotypic 3D collagen I matrix) to form a more structured microenvironment. **b** | Cancer cells of interest are then seeded on top of these fibroblast-contracted organotypic matrices for 1–4 days. **c** | The matrices are then transferred to metal grids. Partially submerged matrices form an air–liquid interface, which provide a chemo-attractive gradient towards the growth medium that promotes cell invasion (see insert). Invading cells can be assessed for paracrine, autocrine or cell type-specific signalling. This can provide higher *in vitro* fidelity to support further *in vivo* drug discovery.

or FRAP, and can be used to examine drug treatment response, track mammary tumour populations or examine cell–cell contact mobility[25,26,54,189,217].

Abdominal imaging windows (AIWs) recently allowed studies of early colonization and micrometastasis formation in the liver[53,218] (FIG. 3). In this case, the authors identified a transient but significant time period, whereby newly extravasated tumour cells showed a rapid mobilization or homing behaviour that was necessary for efficient niche localization, before metastasis formation. Importantly, inhibition of this early mobilization, observed using intravital imaging, was sufficient to block formation of micrometastases[53].

Single cell analysis of drug pharmacokinetics and pharmacodynamics in live animal models has also been demonstrated through semi-automated intravital data analysis[219]. In this case, a thresholding algorithm allowed segmentation of iterated images for a non-biased assessment of drug distribution in cells *in vivo*. Quantification of drug trafficking processes at single cell resolution to visualize intracellular drug exchange has also been achieved using photoactivatable drug-caged fluorophores[220]. In addition, subcellular pharmacokinetic imaging of poly(ADP-ribose) polymerase 1 (PARP1) inhibitors *in vivo* showed that they reached their target (the nucleus) within minutes of administration and at sufficient concentrations[221]. This subcellular detail suggested that drug inefficiency is due to factors other than targeting, such as insensitivity of cancer cells to PARP1 inhibition.

The long-term, high-resolution readouts of drug dynamics that can potentially be achieved using intravital imaging windows from an early disease state (FIG. 3) could also assist in the future design, scheduling and streamlining of effective drug delivery for multiple drug combinations[6,222,223]. This is in line with the recently updated FDA draft guidance that supports further development of novel drug combination strategies[222,223]. A distinct advantage of this longitudinal intravital imaging approach over standard *in vitro* preclinical systems alone is the capacity to monitor drug retention, metabolic turnover and clearance rates in real-time to optimize co-dosing strategies, which could be targeted to influence changes in blood vessel normalization, lymphatic infiltration or drainage, or paracrine or autocrine metabolic feedback signalling from the local microenvironment[212,224–226]. Moreover, this form of repeated intravital imaging may give more reproducible and cost-effective data for the optimization of candidate drugs and combination strategies to guide chemical design within the DPOM (FIG. 1).

Imaging the tumour microenvironment. It is now widely accepted that therapeutic targeting of non-tumour host cells within the tumour microenvironment can contribute to positive therapeutic outcomes[227–229]. Hence, a number of targeted agents against stromal components, including cancer-associated fibroblasts, vascular endothelial cells and inflammatory T cells, have been approved by the FDA or are under clinical development[230–232]. Multiphoton intravital microscopy has been used to directly visualize such tumour or host cell populations within live tumour microenvironments[233–235], extending to real-time monitoring of chemotherapeutic response. One study used GFP-transgenic nude mice (in which all host cells express GFP) and inoculated the spleen with red fluorescent protein (RFP)-expressing human colorectal cancer cells (HT29 cells)[236]. This enabled longitudinal analysis of individual tumour cells in response to changes in both reactive stroma and vascular permeability from within distinct metastatic tissue compartments. Furthermore, the application of real-time stromal imaging to elucidate drug response has recently been demonstrated through an optical window, when sunitinib induced a reduction in overall tumour vascular density and tumour growth but had no major effect on the sprouting behaviour of vascular endothelial cells at the tumour margin[237]. Such data on tumour–host interactions can also be obtained by conventional pathology. However, the use of longitudinal intravital imaging provides more in-depth sampling at multiple timepoints, using fewer animals, providing gains in both statistical robustness and cost compared with conventional immunohistochemical staining.

Intravital imaging studies can also use label-free approaches, such as third harmonic generation imaging (THG imaging; a label-free imaging technique that

Organotypic 3D collagen I matrix
Fibroblast-driven contraction of acid-extracted collagen I is used to produce matrices with high *in vivo* fidelity for analysis of cell behaviour in a live *in vitro* setting.

Multiphoton intravital microscopy
This method reduces interference from the background by using more than one photon as a multiple of the excitation wavelength of the sample, effectively restricting interactions to the focal plane and allowing deep imaging within live tissue.

can be used to assess the interface between aqueous and lipidic structures using multiphoton microscopy). In a recent study, THG was used in parallel with SHG imaging of ECM to track tumour movement in relation to unstained stromal cells and lipid-rich structures, such as adipose tissue[238,239]. Dual imaging in this way revealed invasion routes where cells avoid breaking down ECM components or passing between tight adipose or stromal cells in favour of gaps within the tissue[239]. Importantly, *in vivo* THG imaging also demonstrated the laying down of tumour-associated microparticles, which indicates tumour-imposed conditioning of the local microenvironment[239]. Impairment of this environmental priming or guidance behaviour upon drug treatment may affect tumour invasion efficiency and could potentially be assessed using intravital imaging[225,240].

Many endogenous proteins or live tissues emit an inherent autofluorescent signal. Thus, in a similar manner to monitoring the abundance and activity of exogenous fluorescent biosensors, FLIM can also be used as a label-free method to monitor drug-induced changes on endogenous proteins and biochemical reactions residing within the normal tissue microenvironment[241–243] (FIG. 4). Such an approach can be used to monitor drug-induced changes in tissue physiology, such as pH[244], NADPH[245] or reactive oxygen species (ROS)[199,246–248], which are known to drive distinct processes underlying tumour progression *in vivo*. These studies enable comparative analysis of diseased tissue adjacent to normal tissue or the assessment of systemic liabilities on host tissue biology, such as adverse side effects and toxicities. They can therefore support a new predictive pharmacodynamics approach for drug delivery, retention and target engagement within complex tissue by directly visualizing and quantifying the effects of drugs on normal tissue, relative to intended responses within target tumour tissue.

Current limitations and future directions

Complex 3D model systems that use organic ECM substrates and sophisticated organotypic culture conditions, such as air–liquid interface setups (reviewed in REFS 151,249) (FIG. 2), have limited throughput — taking days to weeks to complete a single study. Such limitations substantially extend the timeline and cost incurred relative to conventional screening assay systems, thereby impeding the broader adoption of such models in drug discovery. However, recent advances in the automation of hanging drop[250–252], collagen matrix[253]

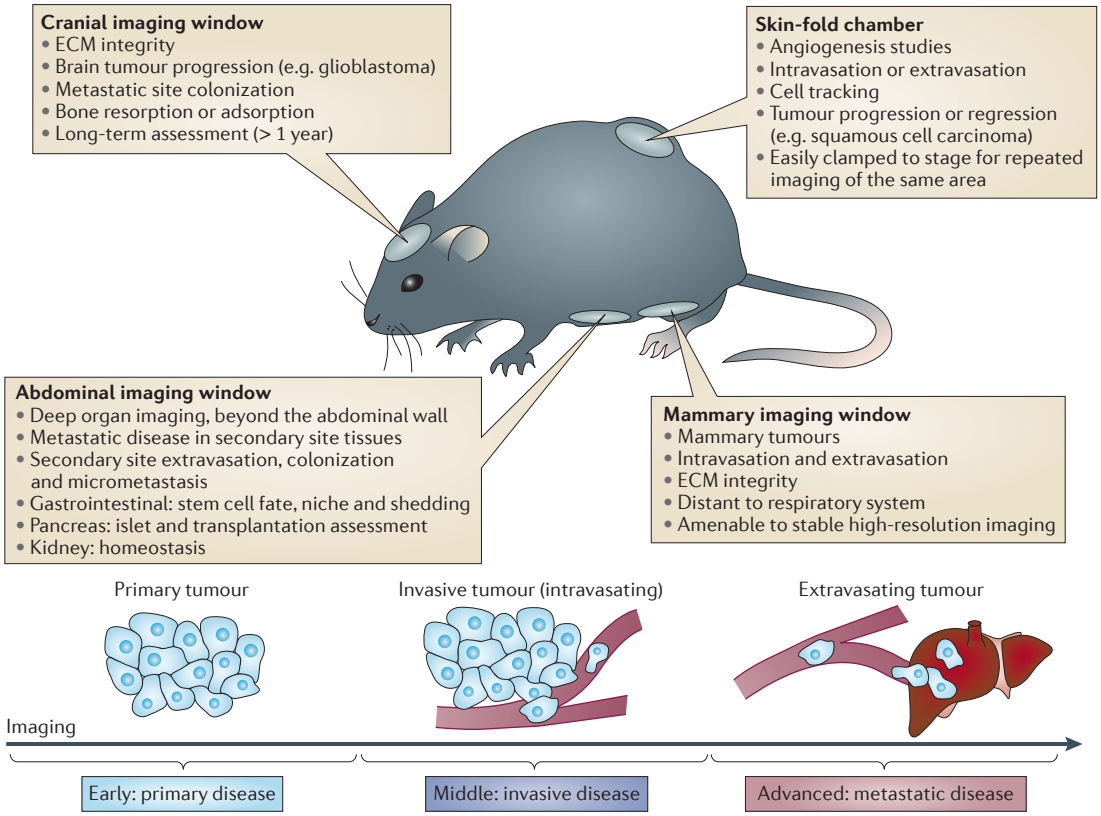

Figure 3 | **Optical imaging windows facilitate non-invasive intravital imaging of drug response in live tissue.** Example optical windows include skin-fold chambers (SFCs), cranial imaging windows (CIWs), mammary imaging windows (MIWs) and abdominal imaging windows (AIWs). The evolving uses of these windows are suggested for each site, some of which include the tracking of tumour cell intravasation or extravasation, angiogenesis studies, xenografts and the observation of micrometastasis in organs that were previously inaccessible to high-resolution, quantitative imaging from deep within the body cavity. Repeated imaging through imaging windows also provides a non-invasive approach to tracking tumour behaviour during early to late stage disease progression or at multiple time-points following drug re-administration. ECM, extracellular matrix.

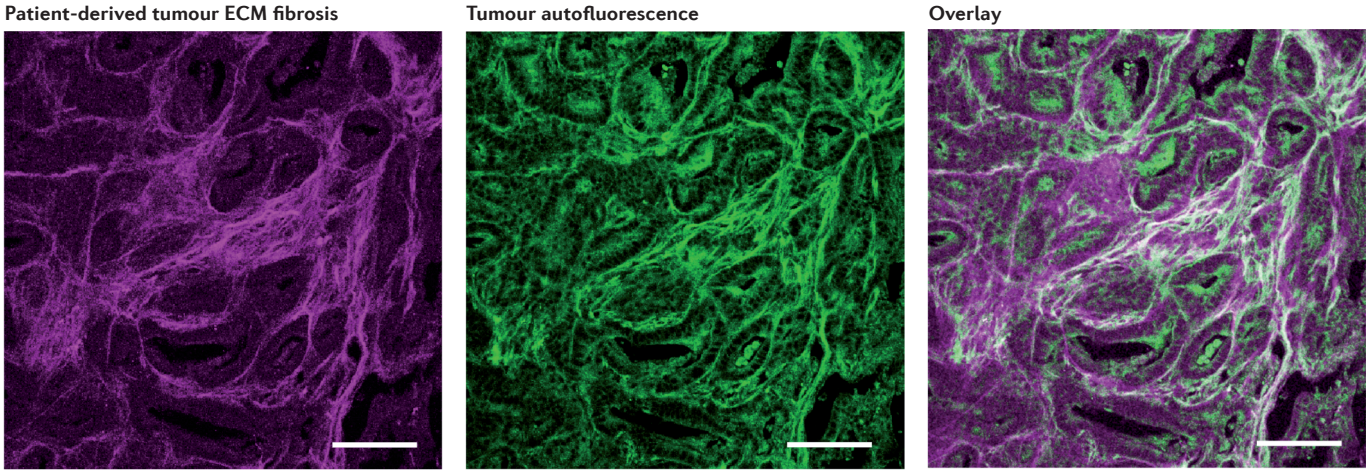

Figure 4 | **Imaging collagen abundance and fibrosis using second harmonic generation microscopy of subcutaneous patient-derived pancreatic tumours.** Purple: collagen signal; green: autofluorescence signal; scale bars: 100 µm; excitation wavelength: 840 nm; second harmonic generation detection range: 400–440 nm; autofluorescence detection range: 500–530 nm. Image obtained using a Leica SP8 multiphoton with coherent compact OPO and time-correlated single photon counting (TCSPC; PicoQuant) fluorescence lifetime imaging microscopy (FLIM) capacity. ECM, extracellular matrix.

and spheroid[254] microplates are joining microfluidics-based systems[255–257] to create uniform 3D microtissues that are suitable for robust automated image-based screening at scale[250].

Despite recent advances, high-resolution intravital imaging in all tissues remains limited by accessibility. The development of stick objective or microprobe lenses facilitates access to specific tissue sites, where imaging is not compatible with standard objective lenses[258]. Further advances in stick objectives include the development of miniaturized fibre optic fluorescent microscopic endoscopic devices, which also have the potential for translation into clinical applications[259]. Such endomicroscopic technology has been further developed to facilitate multidimensional fluorescent imaging and measurement of lifetime within live *in vivo* mouse models or has been used to monitor intestinal integrity in patients[260–262]. Direct multiphoton imaging has also been used to study skin architecture and drug penetrance, as well as melanin and pigmentation levels associated with skin disease in patients and healthy volunteers[263–265]. Such developments of endoscopic or laparoscopic devices, as well as direct multiphoton imaging of patients, may increase the clinical usefulness and statistical robustness of intravital preclinical imaging measurements.

Finally, the biological complexity associated with the metastatic cascade, combined with challenges in carrying out clinical trials of novel anti-metastatic agents, have deterred investment in potentially valuable anti-metastatic drug programmes[266]. Application of 3D tumour invasion models, in conjunction with imaging, is providing detailed mechanistic information on tumour invasion and drug response in distinct microenvironments[152,165,176,267,268]. New genetically engineered mouse and orthotopic transplantation models, as well as experimental models of the later phases of metastatic colonization, are more appropriate for developing anti-metastatic therapy. Hence, new insights into the biology of tumour invasion and metastasis can be gained through intravital imaging at the single cell level[53,215,269,270]. Additionally, there is a crucial need for the drug discovery and microscopy fields to shift their focus towards imaging the processes of micrometastasis formation, as well as tumour growth and survival at metastatic sites, as this is an area that remains poorly understood in the context of intact tissue and one that would greatly benefit from the development of new therapies targeting metastases in cancers that cannot be surgically resected.

In conclusion, we suggest that intravital imaging could be a key enabling technology in the drug discovery process, in which its continued evolution is allowing us to leverage quantitative data from previously unattainable complex settings. Conventional approaches to drug discovery often poorly predict the heterogeneity of response in the clinic, the application of advanced imaging techniques, such as FRAP, FRET, FLIM and photoswitching or photoactivation, facilitates a more unbiased and evidence-led exploration of drug and target mechanisms-of-action across multiple disease settings. These may incorporate the stem cell niche, tumour heterogeneity and tumour–host interactions. Although both target-led and phenotypic image-led models have resulted in the development of many novel and effective medicines, the added value provided by the latest imaging methods remains to be determined. The recent adoption of high-content *in vitro* and repeated *in vivo* imaging within the drug discovery pipeline indicates a willingness to incorporate more complex biology into the discovery process. This may open up new avenues to enhance the success rate of new preclinical-to-clinical translation and improve patient outcome in the long term.

1. Swinney, D. C. The contribution of mechanistic understanding to phenotypic screening for first-in-class medicines. *J. Biomol. Screen* **18**, 1186–1192 (2013).
2. Carragher, N. O. *et al.* Live cell *in vitro* and *in vivo* imaging applications: accelerating drug discovery. *Pharmaceutics* **3**, 141–170 (2011).
3. Timpson, P., McGhee, E. J. & Anderson, K. I. Imaging molecular dynamics in vivo—from cell biology to animal models. *J. Cell Sci.* **124**, 2877–2890 (2011).
4. Paul, S. M. *et al.* How to improve R&D productivity: the pharmaceutical industry's grand challenge. *Nature Rev. Drug Discov.* **9**, 203–214 (2010).
5. Tentler, J. J. *et al.* Patient-derived tumour xenografts as models for oncology drug development. *Nature Rev. Clin. Oncol.* **9**, 338–350 (2012).
6. Kamb, A. What's wrong with our cancer models? *Nature Rev. Drug Discov.* **4**, 161–165 (2005).
7. Weissleder, R. & Pittet, M. J. Imaging in the era of molecular oncology. *Nature* **452**, 580–589 (2008).
8. Beerling, E., Ritsma, L., Vrisekoop, N., Derksen, P. W. & van Rheenen, J. Intravital microscopy: new insights into metastasis of tumors. *J. Cell Sci.* **124**, 299–310 (2011).
9. Lee, J. A. & Berg, E. L. Neoclassic drug discovery: the case for lead generation using phenotypic and functional approaches. *J. Biomol. Screen* **18**, 1143–1155 (2013).
10. Swinney, D. C. & Anthony, J. How were new medicines discovered? *Nature Rev. Drug Discov.* **10**, 507–519 (2011).
This paper reviews the contributions of target- and phenotypic-directed drug discovery in a retrospective analysis of all drugs approved by the FDA between 1999 and 2008.
11. Bakal, C., Aach, J., Church, G. & Perrimon, N. Quantitative morphological signatures define local signaling networks regulating cell morphology. *Science* **316**, 1753–1756 (2007).
12. Vindin, H., Bischof, L., Gunning, P. & Stehn, J. Validation of an algorithm to quantify changes in actin cytoskeletal organization. *J. Biomol. Screen* **19**, 354–368 (2013).
13. Cappella, P. & Gasparri, F. Highly multiplexed phenotypic imaging for cell proliferation studies. *J. Biomol. Screen* **19**, 145–157 (2013).
14. Yarrow, J. C., Totsukawa, G., Charras, G. T. & Mitchison, T. J. Screening for cell migration inhibitors via automated microscopy reveals a Rho-kinase inhibitor. *Chem. Biol.* **12**, 385–395 (2005).
15. Xu, G. W. *et al.* A high-content chemical screen identifies ellipticine as a modulator of p53 nuclear localization. *Apoptosis* **13**, 413–422 (2008).
16. Young, D. W. *et al.* Integrating high-content screening and ligand-target prediction to identify mechanism of action. *Nature Chem. Biol.* **4**, 59–68 (2008).
17. Rose, R. H., Briddon, S. J. & Holliday, N. D. Bimolecular fluorescence complementation: lighting up seven transmembrane domain receptor signalling networks. *Br. J. Pharmacol.* **159**, 738–750 (2010).
18. Dai, J. P. *et al.* Drug screening for autophagy inhibitors based on the dissociation of Beclin1-Bcl2 complex using BiFC technique and mechanism of eugenol on anti-influenza A virus activity. *PLoS ONE* **8**, e61026 (2013).
19. Shinjo, S., Tashiro, E. & Imoto, M. Establishment of a new detection system for the dimerization of IRE1α by BiFC assay. *Biosci. Biotechnol. Biochem.* **77**, 1333–1336 (2013).
20. Filonov, G. S. & Verkhusha, V. V. A near-infrared bifc reporter for in vivo imaging of protein-protein interactions. *Chem. Biol.* **20**, 1078–1086 (2013).
This paper describes the design of the first near-infrared BiFC reporter for *in vivo* protein interaction studies.
21. Fang, D. & Kerppola, T. K. Ubiquitin-mediated fluorescence complementation reveals that Jun ubiquitinated by Itch/AIP4 is localized to lysosomes. *Proc. Natl Acad. Sci. USA* **101**, 14782–14787 (2004).
22. Li, R. *et al.* Akt SUMOylation regulates cell proliferation and tumorigenesis. *Cancer Res.* **73**, 5742–5753 (2013).
23. Day, C. A., Kraft, L. J., Kang, M. & Kenworthy, A. K. Analysis of protein and lipid dynamics using confocal fluorescence recovery after photobleaching (FRAP). *Curr. Protoc. Cytom.* **62**, 2.19.1–2.19.29 (2012).
24. Canel, M., Serrels, A., Anderson, K. I., Frame, M. C. & Brunton, V. G. Use of photoactivation and photobleaching to monitor the dynamic regulation of E-cadherin at the plasma membrane. *Cell Adh. Migr.* **4**, 491–501 (2010).
25. Canel, M. *et al.* Quantitative in vivo imaging of the effects of inhibiting integrin signaling via Src and FAK on cancer cell movement: effects on E-cadherin dynamics. *Cancer Res.* **70**, 9413–9422 (2010).
This paper describes the combined application of intravital imaging windows with three distinct subcellular advanced techniques (photoactivation, photoswitching and FRAP) to examine tumour cell–cell adhesion strength and response to anti-invasive receptor tyrosine kinase (RTK) or endocytic drug treatment.
26. Serrels, A. *et al.* Real-time study of E-cadherin and membrane dynamics in living animals: implications for disease modeling and drug development. *Cancer Res.* **69**, 2714–2719 (2009).
This paper describes the first use of live *in vivo* FRAP to measure cell–cell junction dynamics in living solid tumour tissue: FRAP was used as a surrogate marker of the tumour dissociation response to therapeutic intervention.
27. Yamada, S., Pokutta, S., Drees, F., Weis, W. I. & Nelson, W. J. Deconstructing the cadherin-catenin-actin complex. *Cell* **123**, 889–901 (2005).
28. de Beco, S., Gueudry, C., Amblard, F. & Coscoy, S. Endocytosis is required for E-cadherin redistribution at mature adherens junctions. *Proc. Natl Acad. Sci. USA* **106**, 7010–7015 (2009).
29. Cavey, M., Rauzi, M., Lenne, P. F. & Lecuit, T. A two-tiered mechanism for stabilization and immobilization of E-cadherin. *Nature* **453**, 751–756 (2008).
30. Daddysman, M. K. & Fecko, C. J. Revisiting point FRAP to quantitatively characterize anomalous diffusion in live cells. *J. Phys. Chem. B* **117**, 1241–1251 (2013).
31. Dieteren, C. E. *et al.* Solute diffusion is hindered in the mitochondrial matrix. *Proc. Natl Acad. Sci. USA* **108**, 8657–8662 (2011).
32. Andrews, P. D. *et al.* Aurora B regulates MCAK at the mitotic centromere. *Dev. Cell* **6**, 253–268 (2004).
33. Famulski, J. K. & Chan, G. K. Aurora B kinase-dependent recruitment of hZW10 and hROD to tensionless kinetochores. *Curr. Biol.* **17**, 2143–2149 (2007).
34. Khodjakov, A. & Rieder, C. L. The sudden recruitment of γ-tubulin to the centrosome at the onset of mitosis and its dynamic exchange throughout the cell cycle, do not require microtubules. *J. Cell Biol.* **146**, 585–596 (1999).
35. Vink, M. *et al.* In vitro FRAP identifies the minimal requirements for Mad2 kinetochore dynamics. *Curr. Biol.* **16**, 755–766 (2006).
36. Mueller, F., Wach, P. & McNally, J. G. Evidence for a common mode of transcription factor interaction with chromatin as revealed by improved quantitative fluorescence recovery after photobleaching. *Biophys. J.* **94**, 3323–3339 (2008).
37. Mazza, D., Abernathy, A., Golob, N., Morisaki, T. & McNally, J. G. A benchmark for chromatin binding measurements in live cells. *Nucleic Acids Res.* **40**, e119 (2012).
38. Misteli, T., Gunjan, A., Hock, R., Bustin, M. & Brown, D. T. Dynamic binding of histone H1 to chromatin in living cells. *Nature* **408**, 877–881 (2000).
39. Kang, M., Day, C. A., DiBenedetto, E. & Kenworthy, A. K. A quantitative approach to analyze binding diffusion kinetics by confocal FRAP. *Biophys. J.* **99**, 2737–2747 (2010).
40. Nouar, R., Devred, F., Breuzard, G. & Peyrot, V. FRET and FRAP imaging: approaches to characterise tau and stathmin interactions with microtubules in cells. *Biol. Cell* **105**, 149–161 (2013).
41. Murthy, K. & Wadsworth, P. Dual role for microtubules in regulating cortical contractility during cytokinesis. *J. Cell Sci.* **121**, 2350–2359 (2008).
42. Kraft, L. J. & Kenworthy, A. K. Imaging protein complex formation in the autophagy pathway: analysis of the interaction of LC3 and Atg4B(C74A) in live cells using Forster resonance energy transfer and fluorescence recovery after photobleaching. *J. Biomed. Opt.* **17**, 011008 (2012).
43. Schneider, K. *et al.* Dissection of cell cycle-dependent dynamics of Dnmt1 by FRAP and diffusion-coupled modeling. *Nucleic Acids Res.* **41**, 4860–4876 (2013).
44. Schermelleh, L. *et al.* Dynamics of Dnmt1 interaction with the replication machinery and its role in postreplicative maintenance of DNA methylation. *Nucleic Acids Res.* **35**, 4301–4312 (2007).
45. Spada, F. *et al.* DNMT1 but not its interaction with the replication machinery is required for maintenance of DNA methylation in human cells. *J. Cell Biol.* **176**, 565–571 (2007).
46. Agasti, S. S. *et al.* Dual imaging and photoactivated nanoprobe for controlled cell tracking. *Small* **9**, 222–227 (2013).
47. Wang, X., He, L., Wu, Y. I., Hahn, K. M. & Montell, D. J. Light-mediated activation reveals a key role for Rac in collective guidance of cell movement in vivo. *Nature Cell Biol.* **12**, 591–597 (2010).
48. Yoo, S. K. *et al.* Differential regulation of protrusion and polarity by PI3K during neutrophil motility in live zebrafish. *Dev. Cell* **18**, 226–236 (2010).
49. Frost, N. A., Lu, H. E. & Blanpied, T. A. Optimization of cell morphology measurement via single-molecule tracking PALM. *PLoS ONE* **7**, e36751 (2012).
50. Roy, S., Yang, G., Tang, Y. & Scott, D. A. A simple photoactivation and image analysis module for visualizing and analyzing axonal transport with high temporal resolution. *Nature Protoc.* **7**, 62–68 (2012).
51. Caswell, P. T. *et al.* Rab25 associates with α5β1 integrin to promote invasive migration in 3D microenvironments. *Dev. Cell* **13**, 496–510 (2007).
52. Amornphimoltham, P. *et al.* Rab25 regulates invasion and metastasis in head and neck cancer. *Clin. Cancer Res.* **19**, 1375–1388 (2013).
53. Ritsma, L. *et al.* Intravital microscopy through an abdominal imaging window reveals a pre-micrometastasis stage during liver metastasis. *Sci. Transl Med.* **4**, 158ra145 (2012).
This paper provides an insight into the progressive nature and capacity of intravital imaging windows to monitor late stages of metastasis from deep within the body cavity at high resolution, revealing a time-dependent aspect to when anti-migratory targeting can be effective.
54. Kedrin, D. *et al.* Intravital imaging of metastatic behavior through a mammary imaging window. *Nature Methods* **5**, 1019–1021 (2008).
This paper describes the combined application of intravital imaging windows with photoactivation for repeated imaging and tracking of tumour population dynamics in mammary tumours.
55. Yu, X. *et al.* N-WASP coordinates the delivery and F-actin-mediated capture of MT1-MMP at invasive pseudopods. *J. Cell Biol.* **199**, 527–544 (2012).
56. Deakin, N. O., Ballestrem, C. & Turner, C. E. Paxillin and Hic-5 interaction with vinculin is differentially regulated by Rac1 and RhoA. *PLoS ONE* **7**, e37990 (2012).
This study demonstrates the application of FRET biosensors to provide novel insight into protein–protein interactions within cell adhesions and their distinction between 2D and 3D *in vitro* models.
57. Wouters, F. S., Verveer, P. J. & Bastiaens, P. I. Imaging biochemistry inside cells. *Trends Cell Biol.* **11**, 203–211 (2001).
58. Fruhwirth, G. O. *et al.* How Forster resonance energy transfer imaging improves the understanding of protein interaction networks in cancer biology. *Chemphyschem* **12**, 442–461 (2011).
This is a comprehensive overview of the potential use of FRET-based biosensor imaging in cancer.
59. Seong, J. *et al.* Detection of focal adhesion kinase activation at membrane microdomains by fluorescence resonance energy transfer. *Nature Commun.* **2**, 406 (2011).
60. Wang, Y. *et al.* Visualizing the mechanical activation of Src. *Nature* **434**, 1040–1045 (2005).
61. Hirata, E. *et al.* In vivo fluorescence resonance energy transfer imaging reveals differential activation of Rho-family GTPases in glioblastoma cell invasion. *J. Cell Sci.* **125**, 858–868 (2012).
62. Ouyang, M. *et al.* Visualization of polarized membrane type 1 matrix metalloproteinase activity in live cells by fluorescence resonance energy transfer imaging. *J. Biol. Chem.* **283**, 17740–17748 (2008).
63. Lu, S. *et al.* Quantitative FRET imaging to visualize the invasiveness of live breast cancer cells. *PLoS ONE* **8**, e58569 (2013).
64. Ouyang, M. *et al.* Simultaneous visualization of protumorigenic Src and MT1-MMP activities with fluorescence resonance energy transfer. *Cancer Res.* **70**, 2204–2212 (2010).
This paper describes dual FLIM–FRET imaging of spectrally distinct biosensors for MT1MMP and SRC activity.
65. Luo, K. Q., Yu, V. C., Pu, Y. & Chang, D. C. Application of the fluorescence resonance energy transfer method for studying the dynamics of caspase-3 activation during UV-induced apoptosis in living HeLa cells. *Biochem. Biophys. Res. Commun.* **283**, 1054–1060 (2001).

66. Yoshizaki, H. *et al.* Activity of Rho-family GTPases during cell division as visualized with FRET-based probes. *J. Cell Biol.* **162**, 223–232 (2003).
67. Gavet, O. & Pines, J. Activation of cyclin B1-Cdk1 synchronizes events in the nucleus and the cytoplasm at mitosis. *J. Cell Biol.* **189**, 247–259 (2010).
68. Gavet, O. & Pines, J. Progressive activation of CyclinB1-Cdk1 coordinates entry to mitosis. *Dev. Cell* **18**, 533–543 (2010).
69. Nobis, M. *et al.* Intravital FLIM-FRET imaging reveals dasatinib-induced spatial control of Src in pancreatic cancer. *Cancer Res.* **75**, 4674–4686 (2013).
This paper highlights the usefulness of FRET-biosensor expression in target tissue, providing a reversible and dynamic readout of target inactivation and clearance response to drug treatment in live tumours.
70. Milligan, G. Applications of bioluminescence- and fluorescence resonance energy transfer to drug discovery at G protein-coupled receptors. *Eur. J. Pharm. Sci.* **21**, 397–405 (2004).
71. Tian, H., Ip, L., Luo, H., Chang, D. C. & Luo, K. Q. A high throughput drug screen based on fluorescence resonance energy transfer (FRET) for anticancer activity of compounds from herbal medicine. *Br. J. Pharmacol.* **150**, 321–334 (2007).
72. Stockholm, D. *et al.* Imaging calpain protease activity by multiphoton FRET in living mice. *J. Mol. Biol.* **346**, 215–222 (2005).
73. Janssen, A., Beerling, E., Medema, R. & van Rheenen, J. Intravital FRET imaging of tumor cell viability and mitosis during chemotherapy. *PLoS ONE* **8**, e64029 (2013).
74. Matsuda, T., Horikawa, K., Saito, K. & Nagai, T. Highlighted Ca^{2+} imaging with a genetically encoded 'caged' indicator. *Sci. Rep.* **3**, 1398 (2013).
75. Demarco, I. A., Periasamy, A., Booker, C. F. & Day, R. N. Monitoring dynamic protein interactions with photoquenching FRET. *Nature Methods* **3**, 519–524 (2006).
76. Subach, F. V. *et al.* Red fluorescent protein with reversibly photoswitchable absorbance for photochromic FRET. *Chem. Biol.* **17**, 745–755 (2010).
77. Peter, M. *et al.* Multiphoton-FLIM quantification of the EGFP-mRFP1 FRET pair for localization of membrane receptor-kinase interactions. *Biophys. J.* **88**, 1224–1237 (2005).
78. Talbot, C. B. *et al.* High speed unsupervised fluorescence lifetime imaging confocal multiwell plate reader for high content analysis. *J. Biophoton.* **1**, 514–521 (2008).
This study provides the first example of a FLIM biosensor incorporated into a high-throughput image-based screening platform.
79. Grecco, H. E. *et al.* In situ analysis of tyrosine phosphorylation networks by FLIM on cell arrays. *Nature Methods* **7**, 467–472 (2010).
This paper describes the elegant use of high-speed FLIM to measure FRET in a high-throughput setting, which provides insight into the concerted activity and network redundancy in epidermal growth factor receptor (EGFR) signalling. It is applicable to RTK-targeted drug resistance and feedback.
80. Kumar, S. *et al.* FLIM FRET technology for drug discovery: automated multiwell-plate high-content analysis, multiplexed readouts and application in situ. *Chemphyschem* **12**, 609–626 (2011).
81. Alibhai, D. *et al.* Automated fluorescence lifetime imaging plate reader and its application to Forster resonant energy transfer readout of Gag protein aggregation. *J. Biophoton.* **6**, 398–408 (2013).
82. Grecco, H. E., Roda-Navarro, P., Fengler, S. & Bastiaens, P. I. High-throughput quantification of posttranslational modifications in situ by CA-FLIM. *Methods Enzymol.* **500**, 37–58 (2011).
83. McGhee, E. J. *et al.* FLIM-FRET imaging in vivo reveals 3D-environment spatially regulates RhoGTPase activity during cancer cell invasion. *Small GTPases* **2**, 239–244 (2011).
84. Worth, D. C. & Parsons, M. Advances in imaging cell-matrix adhesions. *J. Cell Sci.* **123**, 3629–3638 (2010).
85. Jares-Erijman, E. A. & Jovin, T. M. FRET imaging. *Nature Biotech.* **21**, 1387–1395 (2003).
86. Berney, C. & Danuser, G. FRET or no FRET: a quantitative comparison. *Biophys. J.* **84**, 3992–4010 (2003).
87. Roh-Johnson, M. *et al.* Macrophage contact induces RhoA GTPase signaling to trigger tumor cell intravasation. *Oncogene* http://dx.doi.org/10.1038/onc.2013.377 (2013).
88. Ottobrini, L., Martelli, C., Trabattoni, D. L., Clerici, M. & Lucignani, G. In vivo imaging of immune cell trafficking in cancer. *Eur. J. Nucl. Med. Mol. Imag.* **38**, 949–968 (2011).
89. Chtanova, T. *et al.* Real-time interactive two-photon photoconversion of recirculating lymphocytes for discontinuous cell tracking in live adult mice. *J. Biophoton* http://dx.doi.org/10.1002/jbio.201200175 (2012).
90. Makrogianneli, K. *et al.* Integrating receptor signal inputs that influence small Rho GTPase activation dynamics at the immunological synapse. *Mol. Cell. Biol.* **29**, 2997–3006 (2009).
91. Lohela, M. & Werb, Z. Intravital imaging of stromal cell dynamics in tumors. *Curr. Opin. Genet. Dev.* **20**, 72–78 (2010).
92. Egeblad, M., Nakasone, E. S. & Werb, Z. Tumors as organs: complex tissues that interface with the entire organism. *Dev. Cell* **18**, 884–901 (2010).
93. Grant, D. M. *et al.* Multiplexed FRET to image multiple signaling events in live cells. *Biophys. J.* **95**, L69–L71 (2008).
94. Rao, J., Bhattacharya, D., Banerjee, B., Sarin, A. & Shivashankar, G. V. Trichostatin-A induces differential changes in histone protein dynamics and expression in HeLa cells. *Biochem. Biophys. Res. Commun.* **363**, 263–268 (2007).
95. Li, W., Wang, Y., Shao, H., He, Y. & Ma, H. Probing rotation dynamics of biomolecules using polarization based fluorescence microscopy. *Microsc. Res. Tech.* **70**, 390–395 (2007).
96. Cao, Z., Huang, C. C. & Tan, W. Nuclease resistance of telomere-like oligonucleotides monitored in live cells by fluorescence anisotropy imaging. *Anal. Chem.* **78**, 1478–1484 (2006).
97. Sharma, P. *et al.* Nanoscale organization of multiple GPI-anchored proteins in living cell membranes. *Cell* **116**, 577–589 (2004).
98. Matthews, D. R. *et al.* A multi-functional imaging approach to high-content protein interaction screening. *PLoS ONE* **7**, e33231 (2012).
99. Eichorst, J. P., Clegg, R. M. & Wang, Y. Red-shifted fluorescent proteins monitor enzymatic activity in live HT-1080 cells with fluorescence lifetime imaging microscopy (FLIM). *J. Microsc.* **248**, 77–89 (2012).
100. Eichorst, J. P., Huang, H., Clegg, R. M. & Wang, Y. Phase differential enhancement of FLIM to distinguish FRET components of a biosensor for monitoring molecular activity of membrane type 1 matrix metalloproteinase in live cells. *J. Fluoresc* **21**, 1763–1777 (2011).
101. Tyas, L., Brophy, V. A., Pope, A., Rivett, A. J. & Tavare, J. M. Rapid caspase-3 activation during apoptosis revealed using fluorescence-resonance energy transfer. *EMBO Rep.* **1**, 266–270 (2000).
102. Shcherbakova, D. M., Hink, M. A., Joosen, L., Gadella, T. W. & Verkhusha, V. V. An orange fluorescent protein with a large Stokes shift for single-excitation multicolor FCCS and FRET imaging. *J. Am. Chem. Soc.* **134**, 7913–7923 (2012).
103. Keese, M., Yagublu, V., Schwenke, K., Post, S. & Bastiaens, P. Fluorescence lifetime imaging microscopy of chemotherapy-induced apoptosis resistance in a syngenic mouse tumor model. *Int. J. Cancer* **126**, 104–113 (2010).
104. Tomura, M. *et al.* Time-lapse observation of cellular function with fluorescent probe reveals novel CTL-target cell interactions. *Int. Immunol.* **21**, 1145–1150 (2009).
105. Yamaguchi, Y. *et al.* Live imaging of apoptosis in a novel transgenic mouse highlights its role in neural tube closure. *J. Cell Biol.* **195**, 1047–1060 (2011).
106. Ting, A. Y., Kain, K. H., Klemke, R. L. & Tsien, R. Y. Genetically encoded fluorescent reporters of protein tyrosine kinase activities in living cells. *Proc. Natl Acad. Sci. USA* **98**, 15003–15008 (2001).
107. Komatsu, N. *et al.* Development of an optimized backbone of FRET biosensors for kinases and GTPases. *Mol. Biol. Cell* **22**, 4647–4656 (2011).
108. Kunkel, M. T., Ni, Q., Tsien, R. Y., Zhang, J. & Newton, A. C. Spatio-temporal dynamics of protein kinase B/Akt signaling revealed by a genetically encoded fluorescent reporter. *J. Biol. Chem.* **280**, 5581–5587 (2005).
109. Sasaki, K., Sato, M. & Umezawa, Y. Fluorescent indicators for Akt/protein kinase B and dynamics of Akt activity visualized in living cells. *J. Biol. Chem.* **278**, 30945–30951 (2003).
110. Yoshizaki, H., Mochizuki, N., Gotoh, Y. & Matsuda, M. Akt-PDK1 complex mediates epidermal growth factor-induced membrane protrusion through Ral activation. *Mol. Biol. Cell* **18**, 119–128 (2007).
111. Mochizuki, N. *et al.* Spatio-temporal images of growth-factor-induced activation of Ras and Rap1. *Nature* **411**, 1065–1068 (2001).
112. Itoh, R. E. *et al.* Activation of rac and cdc42 video imaged by fluorescent resonance energy transfer-based single-molecule probes in the membrane of living cells. *Mol. Cell. Biol.* **22**, 6582–6591 (2002).
113. Kardash, E. *et al.* A role for Rho GTPases and cell-cell adhesion in single-cell motility in vivo. *Nature Cell Biol.* **12** Suppl. 1–11), 47–53 (2010).
114. Timpson, P. *et al.* Spatial regulation of RhoA activity during pancreatic cancer cell invasion driven by mutant p53. *Cancer Res.* **71**, 747–757 (2011).
This study demonstrates that subcellular FLIM–FRET imaging and targeting can reveal subtle but vital signalling events that drive tumour invasion *in vivo*.
115. Goto, A. *et al.* GDNF and endothelin 3 regulate migration of enteric neural crest-derived cells via protein kinase A and Rac1. *J. Neurosci.* **33**, 4901–4912 (2013).
116. Johnsson, A. E. *et al.* The Rac-FRET mouse reveals tight spatiotemporal control of Rac activity in primary cells and tissues. *Cell Reports* **6**, 1153–1164 (2014).
A RAC–FRET biosensor mouse was generated, allowing the spatiotemporal activity of RAC GTPase to be assessed in primary neutrophils and multiple organ types, such as the pancreas, liver, intestine and mammary tissue, in real-time. By crossing this inducible mouse with distinct tumour mouse models, we could expand our knowledge of how RAC GTPase behaves in a native host mammalian tissue upon drug treatment.
117. Fehr, M., Lalonde, S., Lager, I., Wolff, M. W. & Frommer, W. B. In vivo imaging of the dynamics of glucose uptake in the cytosol of COS-7 cells by fluorescent nanosensors. *J. Biol. Chem.* **278**, 19127–19133 (2003).
118. Okumoto, S. *et al.* Detection of glutamate release from neurons by genetically encoded surface-displayed FRET nanosensors. *Proc. Natl Acad. Sci. USA* **102**, 8740–8745 (2005).
119. Imamura, H. *et al.* Visualization of ATP levels inside single living cells with fluorescence resonance energy transfer-based genetically encoded indicators. *Proc. Natl Acad. Sci. USA* **106**, 15651–15656 (2009).
120. Ritsma, L., Vrisekoop, N. & van Rheenen, J. In vivo imaging and histochemistry are combined in the cryosection labelling and intravital microscopy technique. *Nature Commun.* **4**, 2366 (2013).
In this study, in a similar manner to electron microscopy, intravital images were correlated with cryosection labelling to provide post-imaging detail of the sample. Along with instant readouts from intravital imaging, this provides added contextual value and the long-term capacity to re-evaluate the sample after live imaging.
121. Potzkei, J. *et al.* Real-time determination of intracellular oxygen in bacteria using a genetically encoded FRET-based biosensor. *BMC Biol.* **10**, 28 (2012).
This paper describes the development of FluBO, an intramolecular FRET-based biosensor for detecting intracellular oxygen. FluBO uses an oxygen-insensitive donor fluorescent protein that is intramolecularly linked to an oxygen-sensitive acceptor fluorescent protein, and thus FRET only occurs in the presence of oxygen. This biosensor could eventually be applied to measure cellular hypoxia for *in vivo* cancer research.
122. Urra, J. *et al.* A genetically encoded ratiometric sensor to measure extracellular pH in microdomains bounded by basolateral membranes of epithelial cells. *Pflugers Arch.* **457**, 233–242 (2008).
123. Awaji, T., Hirasawa, A., Shirakawa, H., Tsujimoto, G. & Miyazaki, S. Novel green fluorescent protein-based ratiometric indicators for monitoring pH in defined intracellular microdomains. *Biochem. Biophys. Res. Commun.* **289**, 457–462 (2001).
124. Drepper, T. *et al.* Reporter proteins for in vivo fluorescence without oxygen. *Nature Biotech.* **25**, 443–445 (2007).
125. Drepper, T. *et al.* Flavin mononucleotide-based fluorescent reporter proteins outperform green fluorescent protein-like proteins as quantitative in vivo real-time reporters. *Appl. Environ. Microbiol.* **76**, 5990–5994 (2010).
126. Piljic, A. & Schultz, C. Simultaneous recording of multiple cellular events by FRET. *ACS Chem. Biol.* **3**, 156–160 (2008).

127. Peyker, A., Rocks, O. & Bastiaens, P. I. Imaging activation of two Ras isoforms simultaneously in a single cell. *Chembiochem* **6**, 78–85 (2005).
128. Kamioka, Y. *et al.* Live imaging of protein kinase activities in transgenic mice expressing FRET biosensors. *Cell Struct. Funct.* **37**, 65–73 (2012). **This paper describes the generation of FRET biosensor mice.**
129. Nagai, T., Yamada, S., Tominaga, T., Ichikawa, M. & Miyawaki, A. Expanded dynamic range of fluorescent indicators for Ca^{2+} by circularly permuted yellow fluorescent proteins. *Proc. Natl Acad. Sci. USA* **101**, 10554–10559 (2004).
130. Atkin, S. D. *et al.* Transgenic mice expressing a cameleon fluorescent Ca^{2+} indicator in astrocytes and Schwann cells allow study of glial cell Ca^{2+} signals in situ and in vivo. *J. Neurosci. Methods* **181**, 212–226 (2009).
131. Hara, M. *et al.* Imaging endoplasmic reticulum calcium with a fluorescent biosensor in transgenic mice. *Am. J. Physiol. Cell Physiol.* **287**, C932–C938 (2004).
132. Isotani, E. *et al.* Real-time evaluation of myosin light chain kinase activation in smooth muscle tissues from a transgenic calmodulin-biosensor mouse. *Proc. Natl Acad. Sci. USA* **101**, 6279–6284 (2004).
133. Bartoli, M. *et al.* A mouse model for monitoring calpain activity under physiological and pathological conditions. *J. Biol. Chem.* **281**, 39672–39680 (2006).
134. Nikolaev, V. O., Bunemann, M., Schmitteckert, E., Lohse, M. J. & Engelhardt, S. Cyclic AMP imaging in adult cardiac myocytes reveals far-reaching β_1-adrenergic but locally confined β_2-adrenergic receptor-mediated signaling. *Circ. Res.* **99**, 1084–1091 (2006).
135. Calebiro, D. *et al.* Persistent cAMP-signals triggered by internalized G-protein-coupled receptors. *PLoS Biol.* **7**, e1000172 (2009).
136. Sakaue-Sawano, A. *et al.* Visualizing spatiotemporal dynamics of multicellular cell-cycle progression. *Cell* **132**, 487–498 (2008).
137. Yamamoto, N. *et al.* Cellular dynamics visualized in live cells in vitro and in vivo by differential dual-color nuclear-cytoplasmic fluorescent-protein expression. *Cancer Res.* **64**, 4251–4256 (2004).
138. Yamamoto, N. *et al.* Determination of clonality of metastasis by cell-specific color-coded fluorescent-protein imaging. *Cancer Res.* **63**, 7785–7790 (2003).
139. Hoffman, R. M. The multiple uses of fluorescent proteins to visualize cancer in vivo. *Nature Rev. Cancer* **5**, 796–806 (2005).
140. Day, R. N. & Davidson, M. W. Fluorescent proteins for FRET microscopy: monitoring protein interactions in living cells. *Bioessays* **34**, 341–350 (2012).
141. Newman, R. H., Fosbrink, M. D. & Zhang, J. Genetically encodable fluorescent biosensors for tracking signaling dynamics in living cells. *Chem. Rev.* **111**, 3614–3666 (2011).
142. Sahai, E. & Marshall, C. J. Differing modes of tumour cell invasion have distinct requirements for Rho/ROCK signalling and extracellular proteolysis. *Nature Cell Biol.* **5**, 711–719 (2003).
143. Friedl, P. & Wolf, K. Tumour-cell invasion and migration: diversity and escape mechanisms. *Nature Rev. Cancer* **3**, 362–374 (2003).
144. Friedl, P., Sahai, E., Weiss, S. & Yamada, K. M. New dimensions in cell migration. *Nature Rev. Mol. Cell. Biol.* **13**, 743–747 (2012). **This paper gives a comprehensive insight into the appropriate use of 3D matrices to mimic *in vivo* homestasis or disease conditions.**
145. Spence, H. J., Timpson, P., Tang, H. R., Insall, R. H. & Machesky, L. M. Scar/WAVE3 contributes to motility and plasticity of lamellipodial dynamics but not invasion in three dimensions. *Biochem. J.* **448**, 35–42 (2012).
146. Wittig, R. *et al.* Biosensor-expressing spheroid cultures for imaging of drug-induced effects in three dimensions. *J. Biomol. Screen* **18**, 736–743 (2013).
147. le Roux, L. *et al.* Optimizing imaging of three-dimensional multicellular tumor spheroids with fluorescent reporter proteins using confocal microscopy. *Mol. Imag.* **7**, 214–221 (2008).
148. Uchugonova, A. *et al.* Multiphoton tomography visualizes collagen fibers in the tumor microenvironment that maintain cancer-cell anchorage and shape. *J. Cell Biochem.* **114**, 99–102 (2013).
149. Pickl, M. & Ries, C. H. Comparison of 3D and 2D tumor models reveals enhanced HER2 activation in 3D associated with an increased response to trastuzumab. *Oncogene* **28**, 461–468 (2009).
150. Calvo, F. *et al.* Mechanotransduction and YAP-dependent matrix remodelling is required for the generation and maintenance of cancer-associated fibroblasts. *Nature Cell Biol.* **15**, 637–646 (2013).
151. Nurmenniemi, S. *et al.* A novel organotypic model mimics the tumor microenvironment. *Am. J. Pathol.* **175**, 1281–1291 (2009).
152. Gaggioli, C. *et al.* Fibroblast-led collective invasion of carcinoma cells with differing roles for RhoGTPases in leading and following cells. *Nature Cell Biol.* **9**, 1392–1400 (2007). **This paper presents a strong argument for the use of organotypic co-culture models to investigate the complex systems involved in cancer metastasis.**
153. Rothberg, J. M., Sameni, M., Moin, K. & Sloane, B. F. Live-cell imaging of tumor proteolysis: impact of cellular and non-cellular microenvironment. *Biochim. Biophys. Acta* **1824**, 123–132 (2012).
154. Wang, R. *et al.* Three-dimensional co-culture models to study prostate cancer growth, progression, and metastasis to bone. *Semin. Cancer Biol.* **15**, 353–364 (2005).
155. Talukdar, S. & Kundu, S. C. A. non-mulberry silk fibroin protein based 3D in vitro tumor model for evaluation of anticancer drug activity. *Adv. Funct. Mater.* **22**, 4778–4788 (2012).
156. Serebriiskii, I., Castello-Cros, R., Lamb, A., Golemis, E. A. & Cukierman, E. Fibroblast-derived 3D matrix differentially regulates the growth and drug-responsiveness of human cancer cells. *Matrix Biol.* **27**, 573–585 (2008).
157. Loessner, D. *et al.* Bioengineered 3D platform to explore cell-ECM interactions and drug resistance of epithelial ovarian cancer cells. *Biomaterials* **31**, 8494–8506 (2010).
158. Schrader, J. *et al.* Matrix stiffness modulates proliferation, chemotherapeutic response, and dormancy in hepatocellular carcinoma cells. *Hepatology* **53**, 1192–1205 (2011).
159. Sethi, T. *et al.* Extracellular matrix proteins protect small cell lung cancer cells against apoptosis: a mechanism for small cell lung cancer growth and drug resistance in vivo. *Nature Med.* **5**, 662–668 (1999).
160. Longati, P. *et al.* 3D pancreatic carcinoma spheroids induce a matrix-rich, chemoresistant phenotype offering a better model for drug testing. *BMC Cancer* **13**, 95 (2013).
161. Straussman, R. *et al.* Tumour micro-environment elicits innate resistance to RAF inhibitors through HGF secretion. *Nature* **487**, 500–504 (2012). **This study demonstrated that stromal cells conferred innate chemoresistance to cancer cells through treatment with an array of 35 anticancer drugs in 45 cancer cells, cultured alone or in co-culture with stromal cells.**
162. Levental, K. R. *et al.* Matrix crosslinking forces tumor progression by enhancing integrin signaling. *Cell* **139**, 891–906 (2009).
163. Mih, J. D., Marinkovic, A., Liu, F., Sharif, A. S. & Tschumperlin, D. J. Matrix stiffness reverses the effect of actomyosin tension on cell proliferation. *J. Cell Sci.* **125**, 5974–5983 (2012).
164. Zustiak, S., Nossal, R. & Sackett, D. L. Multiwell stiffness assay for the study of cell responsiveness to cytotoxic drugs. *Biotechnol. Bioeng.* **111**, 396–403 (2013).
165. Wolf, K. *et al.* Multi-step pericellular proteolysis controls the transition from individual to collective cancer cell invasion. *Nature Cell Biol.* **9**, 893–904 (2007).
166. Tozluoglu, M. *et al.* Matrix geometry determines optimal cancer cell migration strategy and modulates response to interventions. *Nature Cell Biol.* **15**, 751–762 (2013).
167. Boghaert, E. *et al.* Host epithelial geometry regulates breast cancer cell invasiveness. *Proc. Natl Acad. Sci. USA* **109**, 19632–19637 (2012).
168. Radisky, D. C. & Nelson, C. M. Regulation of mechanical stress by mammary epithelial tissue structure controls breast cancer cell invasion. *Oncotarget* **4**, 498–499 (2013).
169. Jacobetz, M. A. *et al.* Hyaluronan impairs vascular function and drug delivery in a mouse model of pancreatic cancer. *Gut* **62**, 112–120 (2013).
170. Olive, K. P. *et al.* Inhibition of Hedgehog signaling enhances delivery of chemotherapy in a mouse model of pancreatic cancer. *Science* **324**, 1457–1461 (2009). **In this study, SHG imaging reveals that targeting the tumour stromal compartment (ECM) before drug treatment can enhance drug delivery and improve disease outcome. This study led to a shift in the field of dual-targeted therapy in pancreatic cancer.**
171. Provenzano, P. P. *et al.* Enzymatic targeting of the stroma ablates physical barriers to treatment of pancreatic ductal adenocarcinoma. *Cancer Cell* **21**, 418–429 (2012).
172. Yu, M. & Tannock, I. F. Targeting tumor architecture to favor drug penetration: a new weapon to combat chemoresistance in pancreatic cancer? *Cancer Cell* **21**, 327–329 (2012). **References 169 and 172 reveal that alterations in ECM integrity can influence drug targeting via reduced ECM content and improved vascularity or drug delivery.**
173. Raub, C. B., Putnam, A. J., Tromberg, B. J. & George, S. C. Predicting bulk mechanical properties of cellularized collagen gels using multiphoton microscopy. *Acta Biomater.* **6**, 4657–4665 (2010).
174. Samuel, M. S. *et al.* Actomyosin-mediated cellular tension drives increased tissue stiffness and β-catenin activation to induce epidermal hyperplasia and tumor growth. *Cancer Cell* **19**, 776–791 (2011).
175. Cicchi, R. *et al.* Scoring of collagen organization in healthy and diseased human dermis by multiphoton microscopy. *J. Biophoton.* **3**, 34–43 (2010).
176. Bakker, G. J., Andresen, V., Hoffman, R. M. & Friedl, P. Fluorescence lifetime microscopy of tumor cell invasion, drug delivery, and cytotoxicity. *Methods Enzymol.* **504**, 109–125 (2012). **This paper highlights the feasibility of high-speed FLIM–FRET in 3D organotypic or complex settings, allowing cancer cell invasion, apoptosis and drug uptake to be quantified with subcellular resolution.**
177. Bremer, C., Tung, C. H. & Weissleder, R. In vivo molecular target assessment of matrix metalloproteinase inhibition. *Nature Med.* **7**, 743–748 (2001).
178. Contag, P. R. Whole-animal cellular and molecular imaging to accelerate drug development. *Drug Discov. Today* **7**, 555–562 (2002).
179. Graves, E. E., Weissleder, R. & Ntziachristos, V. Fluorescence molecular imaging of small animal tumor models. *Curr. Mol. Med.* **4**, 419–430 (2004).
180. Hoffman, R. M. & Yang, M. Whole-body imaging with fluorescent proteins. *Nature Protoc.* **1**, 1429–1438 (2006).
181. Hayashi, K. *et al.* Real-time imaging of tumor-cell shedding and trafficking in lymphatic channels. *Cancer Res.* **67**, 8223–8228 (2007).
182. Yamauchi, K. *et al.* Development of real-time subcellular dynamic multicolor imaging of cancer-cell trafficking in live mice with a variable-magnification whole-mouse imaging system. *Cancer Res.* **66**, 4208–4214 (2006).
183. Yang, M. *et al.* Direct external imaging of nascent cancer, tumor progression, angiogenesis, and metastasis on internal organs in the fluorescent orthotopic model. *Proc. Natl Acad. Sci. USA* **99**, 3824–3829 (2002).
184. Giampieri, S. *et al.* Localized and reversible TGFβ signalling switches breast cancer cells from cohesive to single cell motility. *Nature Cell Biol.* **11**, 1287–1296 (2009).
185. Li, A. *et al.* Rac1 drives melanoblast organization during mouse development by orchestrating pseudopod- driven motility and cell-cycle progression. *Dev. Cell* **21**, 722–734 (2011).
186. Ladhani, O., Sanchez-Martinez, C., Orgaz, J. L., Jimenez, B. & Volpert, O. V. Pigment epithelium-derived factor blocks tumor extravasation by suppressing amoeboid morphology and mesenchymal proteolysis. *Neoplasia* **13**, 633–642 (2011).
187. Patsialou, A. *et al.* Intravital multiphoton imaging reveals multicellular streaming as a crucial component of in vivo cell migration in human breast tumors. *IntraVital* **2**, e25294 (2013).
188. Ahmed, F. *et al.* GFP expression in the mammary gland for imaging of mammary tumor cells in transgenic mice. *Cancer Res.* **62**, 7166–7169 (2002).
189. Zomer, A. *et al.* Intravital imaging of cancer stem cell plasticity in mammary tumors. *Stem Cells* **31**, 602–606 (2013). **This paper describes the elegant use of simultaneous cell tagging to track cell fate and clonal progeny, and this approach was subsequently used in combination with imaging windows to monitor cell fate in tumour tissue.**

190. Barretto, R. P. *et al.* Time-lapse imaging of disease progression in deep brain areas using fluorescence microendoscopy. *Nature Med.* **17**, 223–228 (2011).
191. Tang, J. C. *et al.* A nanobody-based system using fluorescent proteins as scaffolds for cell-specific gene manipulation. *Cell* **154**, 928–939 (2013).
192. Momiyama, M. *et al.* Imaging the efficacy of UVC irradiation on superficial brain tumors and metastasis in live mice at the subcellular level. *J. Cell Biochem.* **114**, 428–434 (2013).
193. Morton, J. P. *et al.* Mutant p53 drives metastasis and overcomes growth arrest/senescence in pancreatic cancer. *Proc. Natl Acad. Sci. USA* **107**, 246–251 (2010).
This paper describes how whole-body imaging and single cell tagging revealed a role for p53 in outgrowth of senescence, which resulted in tumour progression.
194. Morton, J. P. *et al.* Dasatinib inhibits the development of metastases in a mouse model of pancreatic ductal adenocarcinoma. *Gastroenterology* **139**, 292–303 (2010).
195. Ahmad, I. *et al.* β-Catenin activation synergizes with PTEN loss to cause bladder cancer formation. *Oncogene* **30**, 178–189 (2011).
196. Cole, A. M. *et al.* p21 loss blocks senescence following Apc loss and provokes tumourigenesis in the renal but not the intestinal epithelium. *EMBO Mol. Med.* **2**, 472–486 (2010).
197. Snippert, H. J. *et al.* Intestinal crypt homeostasis results from neutral competition between symmetrically dividing Lgr5 stem cells. *Cell* **143**, 134–144 (2010).
198. Roth, S. *et al.* Paneth cells in intestinal homeostasis and tissue injury. *PLoS ONE* **7**, e38965 (2012).
199. Myant, K. B. *et al.* ROS production and NF-κB activation triggered by RAC1 facilitate WNT-driven intestinal stem cell proliferation and colorectal cancer initiation. *Cell Stem Cell* **12**, 761–773 (2013).
200. Chan, K. T. *et al.* Intravital imaging of a spheroid-based orthotopic model of melanoma in the mouse ear skin. *IntraVital* **2**, e25805 (2013).
201. Lindsay, C. R. *et al.* P-Rex1 is required for efficient melanoblast migration and melanoma metastasis. *Nature Commun.* **2**, 555 (2011).
202. Doyle, B. *et al.* p53 mutation and loss have different effects on tumourigenesis in a novel mouse model of pleomorphic rhabdomyosarcoma. *J. Pathol.* **222**, 129–137 (2010).
203. Gritsenko, P. G., Ilina, O. & Friedl, P. Interstitial guidance of cancer invasion. *J. Pathol.* **226**, 185–199 (2012).
204. Dirat, B. *et al.* Cancer-associated adipocytes exhibit an activated phenotype and contribute to breast cancer invasion. *Cancer Res.* **71**, 2455–2465 (2011).
205. Nieman, K. M. *et al.* Adipocytes promote ovarian cancer metastasis and provide energy for rapid tumor growth. *Nature Med.* **17**, 1498–1503 (2011).
206. Wolf, K. *et al.* Physical limits of cell migration: control by ECM space and nuclear deformation and tuning by proteolysis and traction force. *J. Cell Biol.* **201**, 1069–1084 (2013).
207. Le Devedec, S. E. *et al.* Two-photon intravital multicolour imaging to study metastatic behaviour of cancer cells in vivo. *Methods Mol. Biol.* **769**, 331–349 (2011).
208. Coffey, S. E., Giedt, R. J. & Weissleder, R. Automated analysis of clonal cancer cells by intravital imaging. *IntraVital* **2**, e26138 (2013).
209. Wyckoff, J. *et al.* A paracrine loop between tumor cells and macrophages is required for tumor cell migration in mammary tumors. *Cancer Res.* **64**, 7022–7029 (2004).
210. Wyckoff, J. B. *et al.* Direct visualization of macrophage-assisted tumor cell intravasation in mammary tumors. *Cancer Res.* **67**, 2649–2656 (2007).
211. Lin, E. Y. *et al.* Macrophages regulate the angiogenic switch in a mouse model of breast cancer. *Cancer Res.* **66**, 11238–11246 (2006).
212. Zhou, Z. N. *et al.* Autocrine HBEGF expression promotes breast cancer intravasation, metastasis and macrophage-independent invasion in vivo. *Oncogene* http://dx.doi.org/10.1038/onc.2013.363 (2013).
213. Xu, Z. *et al.* Role of pancreatic stellate cells in pancreatic cancer metastasis. *Am. J. Pathol.* **177**, 2585–2596 (2010).
214. Brown, E. *et al.* Dynamic imaging of collagen and its modulation in tumors in vivo using second-harmonic generation. *Nature Med.* **9**, 796–800 (2003).
215. Kienast, Y. *et al.* Real-time imaging reveals the single steps of brain metastasis formation. *Nature Med.* **16**, 116–122 (2010).
This study demonstrates the use of CIW technology to track metastatic site colonization of cancer cells.
216. Gligorijevic, B. & Condeelis, J. Stretching the timescale of intravital imaging in tumors. *Cell Adh Migr.* **3**, 313–315 (2009).
217. Gligorijevic, B., Kedrin, D., Segall, J. E., Condeelis, J. & van Rheenen, J. Dendra2 photoswitching through the mammary imaging window. *J. Vis. Exp.* **28**, 1278 (2009).
218. Ritsma, L. *et al.* Surgical implantation of an abdominal imaging window for intravital microscopy. *Nature Protoc.* **8**, 583–594 (2013).
This paper describes the application of AIWs to repeatedly and non-invasively monitor organs from deep within the abdominal cavity. Liver, pancreas, intestine and kidney were imaged at high resolution *in situ*.
219. Giedt, R. J., Koch, P. D. & Weissleder, R. Single cell analysis of drug distribution by intravital imaging. *PLoS ONE* **8**, e60988 (2013).
220. Agasti, S. S., Laughney, A. M., Kohler, R. H. & Weissleder, R. A photoactivatable drug-caged fluorophore conjugate allows direct quantification of intracellular drug transport. *Chem. Commun.* **49**, 11050–11052 (2013).
221. Thurber, G. M. *et al.* Single-cell and subcellular pharmacokinetic imaging allows insight into drug action in vivo. *Nature Commun.* **4**, 1504 (2013).
In this study, the authors use intravital imaging to monitor a PARP1 inhibitor reaching its target compartment within the cell *in vivo*.
222. US Department of Health and Human Services. Food and Drug Administration (FDA) Centre for Drug Evaluation and Research (CDER). Guidance for Industry: Codevelopment of two or more new investigational drugs for use in combination. June 2013. Clinical Medicine.
223. Hughes, B. Novel agents combined get own guidance. *Nature Biotech.* **29**, 174 (2011).
224. Natale, D., Soriano, S. F., Coelho, F. M., Hons, M. & Stein, J. V. Comprehensive assessment of quantum dots for multispectral twophoton imaging of dynamic leukocyte migration in lymph nodes. *IntraVital* **2**, e25745 (2013).
225. Suetsugu, A. *et al.* Imaging exosome transfer from breast cancer cells to stroma at metastatic sites in orthotopic nude-mouse models. *Adv. Drug Deliv. Rev.* **65**, 383–390 (2013).
226. Chaudhry, S. I. *et al.* Autocrine IL-1β-TRAF6 signalling promotes squamous cell carcinoma invasion through paracrine TNFα signalling to carcinoma-associated fibroblasts. *Oncogene* **32**, 747–758 (2013).
227. Zhang, J. & Liu, J. Tumor stroma as targets for cancer therapy. *Pharmacol. Ther.* **137**, 200–215 (2013).
228. Bousso, P. & Moreau, H. D. Functional immunoimaging: the revolution continues. *Nature Rev. Immunol.* **12**, 858–864 (2012).
229. Carmeliet, P. & Jain, R. K. Molecular mechanisms and clinical applications of angiogenesis. *Nature* **473**, 298–307 (2011).
230. Mellman, I., Coukos, G. & Dranoff, G. Cancer immunotherapy comes of age. *Nature* **480**, 480–489 (2011).
231. Clarke, J. M. & Hurwitz, H. I. Targeted inhibition of VEGF receptor 2: an update on ramucirumab. *Expert Opin. Biol. Ther.* **13**, 1187–1196 (2013).
232. Di Marco, M., Macchini, M., Vecchiarelli, S., Sina, S. & Biasco, G. Hedgehog signaling: from the cuirass to the heart of pancreatic cancer. *Pancreatology* **12**, 388–393 (2012).
233. Hoffman, R. M. & Yang, M. Color-coded fluorescence imaging of tumor-host interactions. *Nature Protoc.* **1**, 928–935 (2006).
234. Moran, A. E. *et al.* T cell receptor signal strength in Treg and iNKT cell development demonstrated by a novel fluorescent reporter mouse. *J. Exp. Med.* **208**, 1279–1289 (2011).
235. Amoh, Y., Li, L., Katsuoka, K., Bouvet, M. & Hoffman, R. M. GFP-expressing vascularization of Gelfoam as a rapid in vivo assay of angiogenesis stimulators and inhibitors. *Biotechniques* **42**, 294–298 (2007).
236. Tanaka, K. *et al.* In vivo real-time imaging of chemotherapy response on the liver metastatic tumor microenvironment using multiphoton microscopy. *Oncol. Rep.* **28**, 1822–1830 (2012).
237. Manning, C. S. *et al.* Intravital imaging reveals conversion between distinct tumor vascular morphologies and localized vascular response to Sunitinib. *IntraVital* **2**, e24790 (2013).
238. Olivier, N. *et al.* Cell lineage reconstruction of early zebrafish embryos using label-free nonlinear microscopy. *Science* **329**, 967–971 (2010).
239. Weigelin, B., Bakker, G. & Friedl, P. Intravital third harmonic generation microscopy of collective melanoma cell invasion: Principles of interface guidance and microvesicle dynamics. *IntraVital* **1**, 32–43 (2012).
240. Peinado, H. *et al.* Melanoma exosomes educate bone marrow progenitor cells toward a pro-metastatic phenotype through MET. *Nature Med.* **18**, 883–891 (2012).
241. Tadrous, P. J. *et al.* Fluorescence lifetime imaging of unstained tissues: early results in human breast cancer. *J. Pathol.* **199**, 309–317 (2003).
242. Provenzano, P. P., Eliceiri, K. W. & Keely, P. J. Multiphoton microscopy and fluorescence lifetime imaging microscopy (FLIM) to monitor metastasis and the tumor microenvironment. *Clin. Exp. Metastasis* **26**, 357–370 (2009).
243. McGinty, J. *et al.* Wide-field fluorescence lifetime imaging of cancer. *Biomed. Opt. Express* **1**, 627–640 (2010).
244. Estrella, V. *et al.* Acidity generated by the tumor microenvironment drives local invasion. *Cancer Res.* **73**, 1524–1535 (2013).
245. Skala, M. C. *et al.* In vivo multiphoton microscopy of NADH and FAD redox states, fluorescence lifetimes, and cellular morphology in precancerous epithelia. *Proc. Natl Acad. Sci. USA* **104**, 19494–19499 (2007).
246. Lecoq, J. *et al.* Simultaneous two-photon imaging of oxygen and blood flow in deep cerebral vessels. *Nature Med.* **17**, 893–898 (2011).
247. Belousov, V. V. *et al.* Genetically encoded fluorescent indicator for intracellular hydrogen peroxide. *Nature Methods* **3**, 281–286 (2006).
248. Parpaleix, A., Houssen, Y. G. & Charpak, S. Imaging local neuronal activity by monitoring PO^2 transients in capillaries. *Nature Med.* **19**, 241–246 (2013).
249. Timpson, P. *et al.* Organotypic collagen I assay: a malleable platform to assess cell behaviour in a 3-dimensional context. *J. Vis. Exp.* **56**, e3089 (2011).
250. Thoma, C. R. *et al.* A high-throughput-compatible 3D microtissue co-culture system for phenotypic RNAi screening applications. *J. Biomol. Screen* **18**, 1330–1337 (2013).
251. Tung, Y. C. *et al.* High-throughput 3D spheroid culture and drug testing using a 384 hanging drop array. *Analyst* **136**, 473–478 (2011).
252. Drewitz, M. *et al.* Towards automated production and drug sensitivity testing using scaffold-free spherical tumor microtissues. *Biotechnol. J.* **6**, 1488–1496 (2011).
253. Burgstaller, G., Oehrle, B., Koch, I., Lindner, M. & Eickelberg, O. Multiplex profiling of cellular invasion in 3D cell culture models. *PLoS ONE* **8**, e63121 (2013).
254. Truong, H. H. *et al.* Automated microinjection of cell-polymer suspensions in 3D ECM scaffolds for high-throughput quantitative cancer invasion screens. *Biomaterials* **33**, 181–188 (2012).
255. Zervantonakis, I. K. *et al.* Three-dimensional microfluidic model for tumor cell intravasation and endothelial barrier function. *Proc. Natl Acad. Sci. USA* **109**, 13515–13520 (2012).
256. Echeverria, V. *et al.* An automated high-content assay for tumor cell migration through 3-dimensional matrices. *J. Biomol. Screen* **15**, 1144–1151 (2010).
257. Kim, J. *et al.* A programmable microfluidic cell array for combinatorial drug screening. *Lab. Chip* **12**, 1813–1822 (2012).
258. Alencar, H., Mahmood, U., Kawano, Y., Hirata, T. & Weissleder, R. Novel multiwavelength microscopic scanner for mouse imaging. *Neoplasia* **7**, 977–983 (2005).
259. Al-Gubory, K. H. & Houdebine, L. M. In vivo imaging of green fluorescent protein-expressing cells in transgenic animals using fibred confocal fluorescence microscopy. *Eur. J. Cell Biol.* **85**, 837–845 (2006).
260. Kennedy, G. T. *et al.* A fluorescence lifetime imaging scanning confocal endomicroscope. *J. Biophoton.* **3**, 103–107 (2010).
261. Kiesslich, R. *et al.* Identification of epithelial gaps in human small and large intestine by confocal endomicroscopy. *Gastroenterology* **133**, 1769–1778 (2007).

262. Stallmach, A., Schmidt, C., Watson, A. & Kiesslich, R. An unmet medical need: advances in endoscopic imaging of colorectal neoplasia. *J. Biophoton.* **4**, 482–489 (2011).
263. Dancik, Y., Favre, A., Loy, C. J., Zvyagin, A. V. & Roberts, M. S. Use of multiphoton tomography and fluorescence lifetime imaging to investigate skin pigmentation in vivo. *J. Biomed. Opt.* **18**, 26022 (2013).
264. Leite-Silva, V. R. *et al.* The effect of formulation on the penetration of coated and uncoated zinc oxide nanoparticles into the viable epidermis of human skin in vivo. *Eur. J. Pharm. Biopharm.* **84**, 297–308 (2013).
265. Sanchez, W. Y., Obispo, C., Ryan, E., Grice, J. E. & Roberts, M. S. Changes in the redox state and endogenous fluorescence of in vivo human skin due to intrinsic and photo-aging, measured by multiphoton tomography with fluorescence lifetime imaging. *J. Biomed. Opt.* **18**, 061217 (2013).
266. Carragher, N. O. & Frame, M. C. Modelling distinct modes of tumour invasion and metastasis. *Drug Discov. Today Dis. Models* **8**, 103–112 (2011).
267. Sameni, M. *et al.* Imaging and quantifying the dynamics of tumor-associated proteolysis. *Clin. Exp. Metastasis* **26**, 299–309 (2009).
268. Carragher, N. O. Profiling distinct mechanisms of tumour invasion for drug discovery: imaging adhesion, signalling and matrix turnover. *Clin. Exp. Metastasis* **26**, 381–397 (2009).
269. Boimel, P. J. *et al.* Contribution of CXCL12 secretion to invasion of breast cancer cells. *Breast Cancer Res.* **14**, R23 (2012).
270. Xue, C. *et al.* Epidermal growth factor receptor overexpression results in increased tumor cell motility in vivo coordinately with enhanced intravasation and metastasis. *Cancer Res.* **66**, 192–197 (2006).
271. Ai, H. W., Henderson, J. N., Remington, S. J. & Campbell, R. E. Directed evolution of a monomeric, bright and photostable version of Clavularia cyan fluorescent protein: structural characterization and applications in fluorescence imaging. *Biochem. J.* **400**, 531–540 (2006).
272. Markwardt, M. L. *et al.* An improved cerulean fluorescent protein with enhanced brightness and reduced reversible photoswitching. *PLoS ONE* **6**, e17896 (2011).
273. Goedhart, J. *et al.* Bright cyan fluorescent protein variants identified by fluorescence lifetime screening. *Nature Methods* **7**, 137–139 (2010).
274. Goedhart, J. *et al.* Structure-guided evolution of cyan fluorescent proteins towards a quantum yield of 93%. *Nature Commun.* **3**, 751 (2012).
275. Goedhart, J., Vermeer, J. E., Adjobo-Hermans, M. J., van Weeren, L. & Gadella, T. W. Jr. Sensitive detection of p65 homodimers using red-shifted and fluorescent protein-based FRET couples. *PLoS ONE* **2**, e1011 (2007).
276. Aoki, K., Kamioka, Y. & Matsuda, M. Fluorescence resonance energy transfer imaging of cell signaling from in vitro to in vivo: basis of biosensor construction, live imaging, and image processing. *Dev. Growth Differ.* **55**, 515–522 (2013).
277. Truong, K. *et al.* FRET-based in vivo Ca^{2+} imaging by a new calmodulin-GFP fusion molecule. *Nature Struct. Biol.* **8**, 1069–1073 (2001).
278. Miyawaki, A. *et al.* Fluorescent indicators for Ca^{2+} based on green fluorescent proteins and calmodulin. *Nature* **388**, 882–887 (1997).
279. Miyawaki, A., Griesbeck, O., Heim, R. & Tsien, R. Y. Dynamic and quantitative Ca^{2+} measurements using improved cameleons. *Proc. Natl Acad. Sci. USA* **96**, 2135–2140 (1999).
280. Griesbeck, O., Baird, G. S., Campbell, R. E., Zacharias, D. A. & Tsien, R. Y. Reducing the environmental sensitivity of yellow fluorescent protein. Mechanism and applications. *J. Biol. Chem.* **276**, 29188–29194 (2001).
281. Nagai, T. *et al.* A variant of yellow fluorescent protein with fast and efficient maturation for cell-biological applications. *Nature Biotech.* **20**, 87–90 (2002).
282. Evanko, D. S. & Haydon, P. G. Elimination of environmental sensitivity in a cameleon FRET-based calcium sensor via replacement of the acceptor with Venus. *Cell Calcium* **37**, 341–348 (2005).
283. Vinkenborg, J. L., Evers, T. H., Reulen, S. W., Meijer, E. W. & Merkx, M. Enhanced sensitivity of FRET-based protease sensors by redesign of the GFP dimerization interface. *Chembiochem* **8**, 1119–1121 (2007).
284. Ohashi, T., Galiacy, S. D., Briscoe, G. & Erickson, H. P. An experimental study of GFP-based FRET, with application to intrinsically unstructured proteins. *Protein Sci.* **16**, 1429–1438 (2007).
285. Nguyen, A. W. & Daugherty, P. S. Evolutionary optimization of fluorescent proteins for intracellular FRET. *Nature Biotech.* **23**, 355–360 (2005).
286. Lam, A. J. *et al.* Improving FRET dynamic range with bright green and red fluorescent proteins. *Nature Methods* **9**, 1005–1012 (2012).
287. Fritz, R. D. *et al.* A versatile toolkit to produce sensitive FRET biosensors to visualize signaling in time and space. *Sci Signal* **6**, rs12 (2013).
288. Golynskiy, M. V., Rurup, W. F. & Merkx, M. Antibody detection by using a FRET-based protein conformational switch. *Chembiochem* **11**, 2264–2267 (2010).
289. Rehm, M. *et al.* Single-cell fluorescence resonance energy transfer analysis demonstrates that caspase activation during apoptosis is a rapid process. Role of caspase-3. *J. Biol. Chem.* **277**, 24506–24514 (2002).
290. Takemoto, K., Nagai, T., Miyawaki, A. & Miura, M. Spatio-temporal activation of caspase revealed by indicator that is insensitive to environmental effects. *J. Cell Biol.* **160**, 235–243 (2003).
291. Onuki, R. *et al.* Confirmation by FRET in individual living cells of the absence of significant amyloid β-mediated caspase 8 activation. *Proc. Natl Acad. Sci. USA* **99**, 14716–14721 (2002).
292. Li, M., Chen, X., Ye, Q. Z., Vogt, A. & Yin, X. M. A high-throughput FRET-based assay for determination of Atg4 activity. *Autophagy* **8**, 401–412 (2012).
293. Macurek, L. *et al.* Polo-like kinase-1 is activated by aurora A to promote checkpoint recovery. *Nature* **455**, 119–123 (2008).
294. Harvey, C. D. *et al.* A genetically encoded fluorescent sensor of ERK activity. *Proc. Natl Acad. Sci. USA* **105**, 19264–19269 (2008).
295. Mizutani, T. *et al.* A novel FRET-based biosensor for the measurement of BCR-ABL activity and its response to drugs in living cells. *Clin. Cancer Res.* **16**, 3964–3975 (2010).
296. Randriamampita, C. *et al.* A novel ZAP-70 dependent FRET based biosensor reveals kinase activity at both the immunological synapse and the antisynapse. *PLoS ONE* **3**, e1521 (2008).

Acknowledgements
The authors thank H. Bennett, D. Herrmann, A. Magenau, A. Burgess, M. Pajic, B. Browne and C. Vennin. This work was supported by the Australian Research Council (ARC), Cancer Institute New South Wales (CINSW) and National Health and Medical Research Council (NHMRC) funding. N.O.C. is supported by a Research Councils United Kingdom (RCUK) fellowship.

Competing interests statement
The authors declare no competing interests.